



Matthias HÖDL BSc

Investigations of hydration mechanisms and early compressive strength development of dry- mix shotcrete

MASTER THESIS

To obtain the academic degree
Diplom-Ingenieur
of
Civil Engineering Sciences and Structural Engineering

Graz University of Technology

Faculty of Civil Engineering

Institute of Technology and Testing of Construction Materials

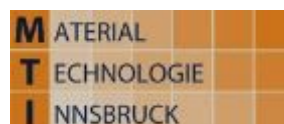
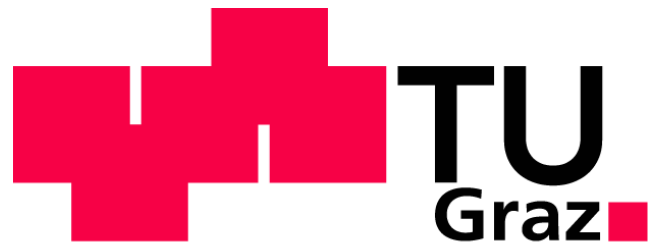
Supervisor:

Mag. rer. nat. Dr. rer. nat. Florian MITTERMAYR

Dipl.-Ing. Lukas BRIENDL BSc

Graz, March 2019

In cooperation with:



EIDESSTATTLICHE ERKLÄRUNG

Ich erkläre an Eides statt, dass ich die vorliegende Arbeit selbstständig verfasst, andere als die angegebenen Quellen/Hilfsmittel nicht benutzt und die den benutzten Quellen wörtlich und inhaltlich entnommene Stellen als solche kenntlich gemacht habe.

Graz, am

.....
(Unterschrift des Studenten)

STATUTORY DECLARATION

I declare that I have authored this thesis independently, that I have not used other than the declared sources / resources, and that I have explicitly marked all material, which has been quoted either literally or by content from the used sources.

.....
(Date)

.....
(Signature)

Danksagung

An dieser Stelle möchte ich allen Personen danken, die mir während der Erstellung meiner Diplomarbeit mit Rat und Tat zur Seite standen. Insbesondere möchte ich mich für die Betreuung von universitärer Seite bei Herrn Florian Mittermayr und bei Herrn Lukas Briendl bedanken. Vielen Dank, dass Sie mir die Gelegenheit gegeben haben, bei Ihnen zu forschen und zu arbeiten. Durch Ihre fundierte Expertise im Bereich der Betontechnologie konnten Sie mich bei meinen Recherchen und Fragen unterstützen. Ihre konstruktive Kritik verhalf mir zu einer durchdachten These und Fragestellung.

Des Weiteren, entstand diese Arbeit in enger Zusammenarbeit mit den wissenschaftlichen Mitarbeitern und zahlreichen Industriepartnern des FFG Collective Research Forschungsprojekts „ASSpC“. Ohne sie wäre diese Arbeit in dieser Form nicht möglich gewesen.

Ein ganz besonderer Dank gebührt meinen Eltern, Alois und Veronika, die mich während meiner gesamten Ausbildungszeit hindurch unterstützten und mit Rat und Tat zu allen Zeiten zur Seite standen. Ohne sie hätte ich diese Zeilen nie geschrieben.

Graz, am Dienstag, 24. März 2019

.....
(Unterschrift des Studenten)

Kurzfassung

Im Vorfeld der gegenständlichen Masterarbeit wurden im Rahmen eines Großspritzversuches, Druckfestigkeitsuntersuchungen von zuvor ausgewählten Trockenspritzbeton- Rezepturen durchgeführt. Anschließend wurden die verwendeten Rezepturen im Labor reproduziert und die Druckfestigkeit abermals bestimmt. Dazu wurden prismatische Probekörper aus Trockenspritzbeton entsprechend den Mischungsentwürfen hergestellt. In den anschließenden Auswertungen wurden die Laborergebnisse der Druckfestigkeitsuntersuchungen mit jenen Ergebnissen des Großspritzversuches verglichen.

Im darauf folgenden Schritt erfolgte die Untersuchung der thermodynamischen Hydratationsvorgänge, welche während der chemischen Reaktion von Wasser mit Zement, Zusatzstoffen und Zusatzmitteln vonstattengehen. Dazu wurden frische Mischungen mit einem isothermen Kalorimeter während eines Zeitraums von 24 Stunden beobachtet. Das Ziel dieser Untersuchungen war es den Einfluss von Zusatzstoffen auf die Reaktionsverläufe, und in weiterer Folge auf die Hydrationsmechanismen und die Druckfestigkeit, zu beobachten.

In einem letzten Schritt wurden die Phasenumwandlungen während der Hydratation an Hand ausgewählter Mischungen mittels Röntgenstrukturanalyseverfahren über einen Zeitraum von 24 Stunden beobachtet. Dazu wurde zum einen der Einfluss eines, in geringen Maßen vorhandenen, Calcium-Sulfat-Anteiles beobachtet. Zum anderen wurde der Effekt eines Calciumaluminatzementes, auf die Phasenumwandlung untersucht.

Zusätzlich zu den zuvor genannten Untersuchungen wurde die Korrelation der Reaktionswärme- und Druckfestigkeitsentwicklung untersucht. Die dadurch errungen Erkenntnisse können zukünftig dazu genutzt werden, um die Druckfestigkeitsuntersuchungen von Trockenspritzbeton zu beschleunigen und die noch zu erreichende Druckfestigkeit zu prognostizieren.

Schlagwörter: Hydratation, Trockenspritzbeton, Kalorimetrie, Druckfestigkeit, Hydratationswärme, Anfangshydratation, Hydratationsmechanismen, Röntgenstrukturanalyse

Abstract

The first step of this master thesis was to investigate the compressive strength development of pre-selected dry-mix shotcrete mixtures, which were sprayed during the in-situ full-scale test. Therefore, test specimens of dry-mix shotcrete mortar were produced accordingly to mixtures from the full-scale test. These samples were tested concerning their compressive strength development. The results were then compared with the outcomes of the full-scale test.

The next step was to determine the heat release, which occurs through the chemical reaction of water, cement, other supplementary cementitious materials and admixtures with an isothermal calorimeter during the first 24 hours. The aim of this investigation was to show the effects of supplementary cementitious materials on the reaction process and on the mechanisms of hydration.

In a final step, the phase assemblage evolution during hydration of preselected mixtures was observed through an in-situ X-ray diffraction over a period of 24 hours. Therefore, the effects of very low amounts of available calcium sulphate in the mixtures, which is a major feature of dry-mix shotcrete in Austria, were observed. Moreover, the effects of calcium aluminate cement as an additional cementitious material in the mixtures were detected.

In addition to that, correlation studies of the heat release and the compressive strength development of prisms made of dry-mix shotcrete mortar were implemented. This research was conducted to gain a better understanding of the dependency between the chemical reaction of cement with water, supplementary cementitious materials and admixtures. The accomplishments of this research can be applied for an initial and fast estimation of the compressive strength development of a dry-mix shotcrete afterwards.

Keywords: Hydration, Dry-mix Shotcrete, Calorimetry, Compressive Strength, Heat Release, Heat of Hydration, Early-age Hydration, Mechanisms of Hydration

Index of Abbreviations

A	Al_2O_3	Aluminium Oxide
Ai		Passing Fraction
AFm	$\text{C}_3\text{A}(\text{Cs})\text{H}_{12}$	Monosulphate
AFmc	$\text{C}_3\text{ACaCO}_3\cdot 11\text{H}_2\text{O}$	Monocarbonate
AFt	$\text{C}_3\text{A}(\text{Cs})_3\text{H}_{32}$	Ettringite
BET		Brunauer-Emmett-Teller theory
C	CaO	Calcium Oxide
C_2S	Ca_2SiO_4	Dicalcium Silicate or Belite
C_3S	Ca_3SiO_5	Tricalcium Silicate or Alite
C_3A	$\text{Ca}_3\text{Al}_2\text{O}_6$	Tricalcium Aluminate or Aluminate
C_4AF	$\text{Ca}_2\text{AlFeO}_5$	Tetracalcium Aluminoferrite or Ferrite
CA		Monocalcium Aluminate
CAC		Calcium Aluminate Cement
CAH		Calcium Aluminate Hydrate
CS		Compressive Strength
cf.		Compare
CH	$\text{Ca}(\text{OH})_2$	Calcium Hydroxide or Portlandite
CSH		Calcium Silicate Hydrate
d_j		mesh size
D_{max}		largest grain size
F	Fe_2O_3	Ferrous Oxide
FST		Full-Scale Test
GGBFS		Ground granulated blast furnace
ΔH_{R}		Enthalpy of reaction
H	H_2O	Water
MIF		Micro-filler
MK	$\text{Al}_2\text{Si}_2\text{O}_7$	Metakolin
OPC		Ordinary Portland Cement
ÖBV		Österreichische Bautechnik Vereinigung
Q		Heat energy
REF		Reference
S	SiO_2	Silicon Dioxide
SCM		Supplementary Cementitious Material
ΔU		inner Energy
W		Work
W/B		Water to Binder ratio
W/C		Water to Cement ratio
XRD		X-ray Diffraction

Greek letters:

α	alpha
β	beta
γ	gamma
θ	theta
λ	lambda

0 Contents

1	Introduction and Aims	8
1.1	Procedure	9
2	Theoretical Principles	10
2.1	Dry-mix Shotcrete	10
2.1.1	Reactions of Cement with Water in regard to Dry-mix Shotcrete.....	10
2.1.2	Hydration Mechanisms of Dry-mix Shotcrete	13
2.1.3	Heat of Hydration	15
2.1.4	Influences on Hydration, Setting and Hardening Procedure.....	16
2.2	Properties of Supplementary- Cementitious Materials and Admixtures.....	16
2.2.1	Ground Granulated Blast Furnace Slag.....	17
2.2.2	Metakaolin	17
2.2.3	Calcium Aluminate Cement.....	17
2.2.4	Limestone Powder	18
2.2.5	Aggregate	19
2.3	Calorimetry.....	20
2.3.1	Basics of Thermodynamic Reactions	20
2.3.2	Isothermal Calorimetry	21
2.4	X-ray Diffraction (XRD).....	22
2.4.1	Data Analyses.....	23
3	Experimental Arrangements	25
3.1	Raw Materials.....	26
3.2	Full-Scale Test	28
3.2.1	Aggregates for the Dry-mix shotcrete of the Full-Scale Test.....	28
3.2.2	Recipes	29
3.2.3	Compressive Strength Results	29
3.3	Laboratory Tests.....	31
3.3.1	Raw Material and Recipes.....	31
3.3.2	Aggregate of Dry-mix Mortar for Laboratory Tests	32
3.3.3	Mixing Procedure	33
3.3.4	Bending Tension- (BT) and Compressive-strength-Test (CS)	33
3.3.5	Calorimetry	35
3.3.6	X-ray Diffraction (XRD).....	35
4	Experimental Results	37
4.1	Strength Development of Dry-mix Shotcrete	37

4.1.1	Compressive Strength of Series W2-03 to W2-14.....	37
4.1.2	Compressive Strength of Series REF1 and REF2	38
4.2	Calorimetry.....	39
4.3	XRD.....	45
4.3.1	XRD-Investigations of REF1.....	45
4.3.2	XRD-Investigations of REF2.....	47
5	Analysis and Argumentation	49
5.1	Compressive Strength Development under Laboratory Conditions.....	49
5.1.1	Laboratory - versus Full-Scale Test	50
5.2	Calorimetry.....	52
5.2.1	Correlation: Heat Release – Compressive Strength.....	54
5.3	XRD.....	56
6	Conclusion	58
	List of literature	60
	List of Illustration	63
	List of Tables	65
	Appendix A.....	66
	Appendix B	68
	Appendix C	73

1 Introduction and Aims

The concrete- and especially shotcrete -technology in combination with the “New Austrian Tunnelling Method” (NATM) has become the standard technology in tunnelling and underground mining worldwide for more than 50 years, cf. (Poso and Windshügel 2014). Regarding this, shotcrete is a mostly hidden but very important construction material. It is a physical safeguarding measure during construction work in building pits and tunnels. Furthermore, shotcrete is used as a rock support and a fixed component of tunnel linings. Depending on the specific challenges, shotcrete takes over rock pressure, prevents from water inlet or protects miners from rock bursts during the construction phase.

In general, there are two different procedures of applying shotcrete on a surface. These methods are called wet-and dry-mix shotcrete. The most obvious difference between these two types is the mixing process. Wet-mix shotcrete is a ready-made concrete, which is pumped through a hose to the nozzle. It is the most commonly used procedure when a high performance is necessary. Though, it is not very flexible in respect to layoffs.

In contrast, dry-mix shotcrete is cement, which is mixed with a set accelerator and water right at the nozzle, which is the most frequently used dry-mix method. The dry-mix shotcrete is either premixed oven-dry or adhesive moist powder. This powder is pumped with compacted air through a hose to the nozzle. The mixing water and, if necessary, fluid admixtures are added at the nozzle. Figure 1 shows a schematic illustration of the dry-mix procedure. The addition of water right at the nozzle leads to a greater operating range. Layoffs are possible, which are convenient in unexpected fault zones during mining. Moreover, lower water to binder ratios are possible, which are a major parameter in depending on stiffness and strength development. In addition to previously notified shotcretes, there have been developed cements without set accelerators in Austria in the 1990s. They contain none or just a very small quantity of calcium sulphate, which lead to a very rapid reaction with water and within to a very rapid setting. These binders are regulated in “ÖVBB-Richtlinie Spritzbeton”, cf. (Österreichische Bautechnik Vereinigung 2009) and cf. (Poso and Windshügel 2014, 363–70). In this current work, they are abbreviated “SPBM”.

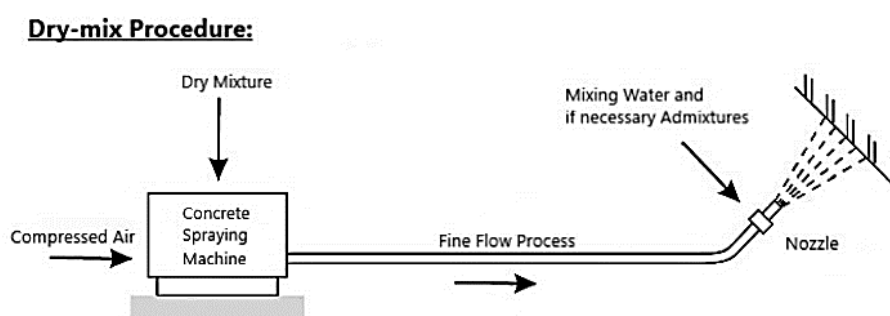


Figure 1: Dry-mix procedure, adapted from (Ruffert, Brux, and Badzong 1995)¹

Nowadays, the environmental aspects and lifecycle costs of a structure became more important. Nonetheless, studies showed that the presence of mountain water rich in sulphate or chloride, as well as the high amount of CO₂ in the surrounding tunnel environment, weaken the concrete-structure and leads to a leaching process (Wegmüller 2001). These leaching process is a major problem for the drainage system of a tunnel. Moreover, infrastructures such as tunnel are designed and built to remain at least

¹ (Ruffert, Brux, and Badzong 1995, 25)

120 to 200 years. Such a long lifespan leads to tremendously high repair and maintenance costs for society. Seventy-five percent of all costs of maintenance are caused by draining water arising in a tunnel, cf. (Kusterle 2006, 87–103).

According to the risky and challenging long service life of such infrastructure projects, there is ongoing research to improve existing technology and to find new methods to fulfil those environmental requirements. Thus, it is necessary to have a very well understanding of all kinds of chemical attacks, the hydration process and the internal structure of shotcrete to accomplish these requirements.

Therefore, the project ASSpC (Advanced and Sustainable Sprayed Concrete) at the Graz University of Technology, the OTH Regensburg and the material technology university Innsbruck in cooperation with the "Österreichische Bautechnikveranstaltungs GmbH" (ÖBV GmbH) has been initialised. This project has three main targets that are:

- the development of new shotcrete recipes
- the improvement of shotcrete durability
- the advanced apprehensions of shotcrete

According to that, the aim of this master thesis is to show the correlation of strength development, heat release and phase assemblage evolution during hydration of dry-mix shotcrete caused by the chemical reactions of water with cement and/or other binder materials. This assumption shall exhibit the relationship between a rising setting, early-age strength development, and an increasing amount of energy over time. Further, this work should help to speed up the testing procedure of the early-age compressive strength testing of dry-mix shotcrete-blends under laboratory conditions. Eventually, this thesis should help to add clarity to the hardly researched hydration process of dry-mix shotcrete.

1.1 Procedure

The starting point of this master thesis was the full-scale test of dry-mix shotcrete at the cement plant of w&p in Wietersdorf during the time of 12th to 16th of March 2018. A preselected collection of different mixes was tested under realistic conditions. The mixtures with the most promising results were selected afterwards for further investigations. These investigations included following examination steps.

- Investigations of the early strength development.
- Observations of chemical reaction of mixtures with a calorimeter during the first 24 hours of hydration
- Detailed examinations of two mixtures through an x-ray diffraction with Rietveld analyses

2 Theoretical Principles

This study deals with dry-mix shotcrete, a specific topic in the field of civil engineering. To ensure a better understanding, the following subchapters give a brief introduction to the basics of dry-mix shotcrete with a focus on mechanisms at a very early age of hydration.

2.1 Dry-mix Shotcrete

In general, dry-mix shotcrete is a product, which is formed through inorganic chemical- and physico-mechanical reactions of anhydrous compounds with water. This process is generally known as hydration and the major constituents are water and cement.

2.1.1 Reactions of Cement with Water in regard to Dry-mix Shotcrete

Cement in general is made by heating a mixture of calcium oxide (CaO), silicon dioxide (SiO₂), smaller amounts of aluminium oxide (Al₂O₃) and ferrous oxide (Fe₂O₃) to a temperature of approximately 1450°C. Because of this high temperature, a sintering occurs, and clinker is generated. It is a composite of around 67% CaO, 22% SiO₂, 5% Al₂O₃, 3% Fe₂O₃ and 3% other components. The clinker contains four major phases, which are Alite **C₃S** (tricalcium silicate or Ca₃SiO₅), Belite **C₂S** (dicalcium silicate or Ca₂SiO₄), Aluminate **C₃A** (tricalcium aluminate or Ca₃Al₂O₆) and Ferrite **C₄AF** (tetracalcium aluminoferrite or Ca₂AlFeO₅). (Taylor 2003, 1–2) The setting process results from exothermic reactions of water with these four major phases. Figure 2 shows this hydration rate by time. It is recognizable that the hydration of C₃A and C₄AF is very high at the beginning in comparison with C₃S and C₂S, based on the condition that sulphate is rarely available.

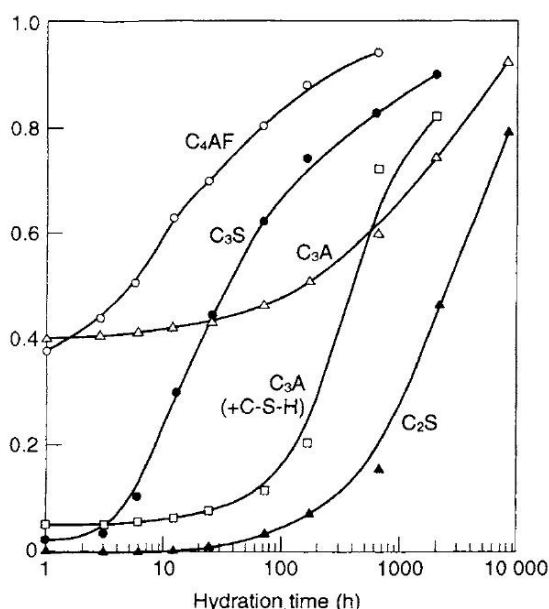
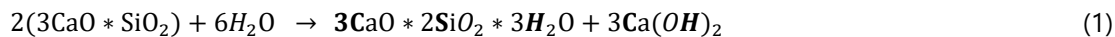


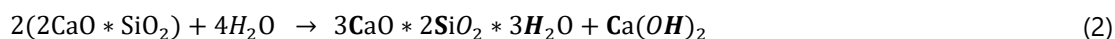
Figure 2: Typical hydration kinetics of pure clinker minerals (C₃A without and with added gypsum)²

² (Hewlett and Lea 2001)

The most important clinker-phase for Ordinary Portland Cement (OPC) is the alite. It reacts relatively quickly, and is essential in terms of early (from the first hour on) and late strength development. The pure reaction of C_3S with water is a rather complex reaction, and it is still not fully understood. At ambient temperature amorphous calcium silicate hydrate (CSH) with a CaO/SiO_2 ratio of less than 3.0 and crystalline calcium hydroxide also known as portlandite (CH) is formed cf. (Hewlett and Lea 2001, 243).

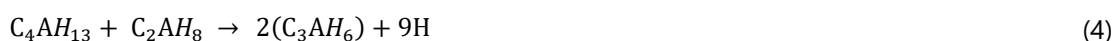
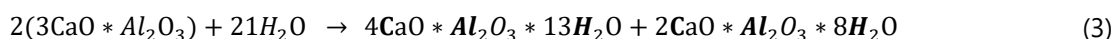


Equation (1) shows the reaction of C_3S and water. The progress of this reaction can be described by the rate of hydration, which can be studied by determining the amount of non-reacted crystalline C_3S through a XRD-analysis. The belite reacts similarly with water but slower and more constantly than the alite. Therefore, C_2S influences the strength development significantly at a later stage. This is mainly caused by its lower solubility in water. As it is shown in (2), CSH and CH occur.



Through the hydration processes, needle-shaped CSH-phases cover the clinker grains. These CSH-phases grow against the free pore space, where they interlock each other and build a solid structure. The CSH-phases occur in cement in different ways. It depends on the water content between the CaO - and SiO_2 -layers. In a more detailed perspective, the CSH appears between the two borders $C_5S_6H_9$ (tobermorite) and $C_9S_6H_{11}$ (jennite), for example as C_2SH (hillebrandite), $C_2S_3H_2$ (gyrolite), $C_3S_2H_3$ (afwillite), C_4S_3H (foshagite) and C_6S_6H (xonotlite). The formation of CSH depends on a number of different parameters. The most important ones are w/c-ratio, temperature, grinding fineness and the presence of additional supplementary cementitious materials containing silica cf. (Benedix 2015, 353–54).

Aluminate and Ferrite react with water very rapidly. Especially aluminate is important for the setting development in the first few minutes. Both are very sensitive to calcium sulphate. The absence of sulphate during the reaction of C_3A with water leads to an instant setting and a high exploration of heat energy. C_4AH_{13} and C_2AH_8 occurs in a first step, see equation (3). These calcium aluminate hydrates (CAH) shape crystals and form a chart house like structure, which leads to a setting of the cement-water mixture right after combining them. The instable calcium aluminate hydrates converts afterwards to C_3AH_6 (katoite) cf. (4).



On the contrary, the presence of small amounts (about five percent) calcium sulphate $CaO_4 * xH_2O$ ($C\$H_x$) act as a set-controlling agent during the reaction of C_3A with water. The amount of $C\$H_x$ influences the chemical reactions and their outcome. A high amount of $C\$H_x$ in combination with C_3A and water forms Ettringite (AFt-phase), cf. (5).



When the entire $C\$H_x$ has been consumed, and there is some C_3A left, the C_3A is going to react with the trisulphate and water to monosulphate (AFm- phase) which containing less sulphate.

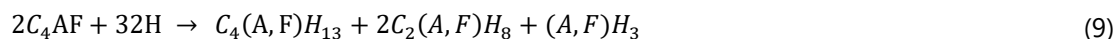


In case of a very low concentration of sulphate in the solution, AFm is formed instead of AFt, see equation (8). (Stark and Wicht 2000, 192) indicates the formation of AFt and AFm depending on the C_sH_2/C_3A -ratio, cf. Table 1.

C_sH_2/C_3A	Reaction product:
>3.0	AFt and free gypsum
3.0	AFt
1.0 – 3.0	AFt and AFm
1.0	AFm
<1.0	AFm and C_4AH_{13} , C_2AH_8 , or $C_3A(Cs,CH)H_{12}$
0	C_3AH_6

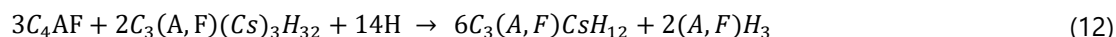
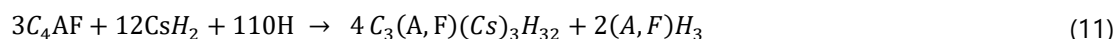
Table 1: C_3A/C_sH_2 -ratio and predicted reaction products

There has been little research on the hydration of tetracalcium aluminoferrite so far. In general it is supposed, that C_4AF reacts similarly but slower than the C_3A , (Taylor 2003). In absence of sulphate, the instable ferrite phases $C_4(A,F)H_{13}$, $C_2(A,F)H_8$, a mix of iron(III)-hydroxide $Fe(OH)_3$ and aluminate-hydroxide $Al(OH)_3$ arises. The Ferrite-phases decompose in $C_3(A,F)H_6$ and water, as it is shown in (9) and (10), afterwards.



This swift reaction of C_3A with water is used for dry-mix shotcrete. The setting process starts rather immediately, and an additional accelerator is not necessary.

If sulphate is present, aluminate- trisulphate $C_3(A,F)(Cs)_3H_{32}$ is formed. This aluminate-trisulphate converts, as shown in (11) and (12), to monosulphate $C_3(A,F)CsH_{12}$.



In general, dry-mix shotcrete consists of a cement, a sprayable binding agent, with a low content of sulphate in comparison with OPC. This low amount of sulphate leads to a very rapid setting in cement or shotcrete pasts and an additional accelerator is not necessary, cf. (Springenschmid 2007, 37). The amount of sulphate

However, the speed of hydration is not only influenced by the available clinker-phases, but also through the speed of cooling during the clinker production, defects in the crystal lattice, size of crystals and the presence of external oxides (for example K_2O and Na_2O). Further, the grinding fineness, the w/c-ratio, ambient temperature and the mixing manner and time influence the manner of reaction in an indirectly way, cf. (Verein Deutscher Zementwerke 2008).

2.1.2 Hydration Mechanisms of Dry-mix Shotcrete

The hydration of cement at ambient temperature is characterised by four different periods. These periods are described in detail in the following paragraphs. The hydration mechanisms and within the setting behaviour of dry-mix shotcrete is influenced significantly by the presence or absence of calcium sulphate.

Pre- induction period

Immediately after the contact of cement with water, swift and very intense reactions evolves. An intense liberation of heat energy can be observed as well, at this stage of hydration. Alkali sulphates, which are present in cement, dissolve in H_2O within seconds. C_3S dissolves similarly, and because of this reaction, CSH phases precipitate at the surface of the cement particle. This reaction is accompanied by an increase of Ca^{2+} and OH^- -ion- concentration in the liquid phase. In addition to that, silicate ions enter the liquid phase, even though their concentration is very low.

The reaction of cement with water is highly infected by the presence or absence of calcium sulphate. The presence of small quantities (up to five percent) of calcium sulphate, which is typical for OPC, lead to a reaction with C_3A . A gel-like material occur at the C_3A -surface. This gel transforms slowly into long shaped crystals (AFt). cf. (Taylor 2003, 265–66). In absence (or in presence of very small quantities) of calcium sulphate, C_3A reacts quickly with water and hexagonal crystals, in the form of C_2AH_8 or C_4AH_{19} , grow on the C_3A -surface. These hexagonal crystals build bridges between cement particles and a setting occurs. This effect is exploit in terms of dry-mix shotcrete (in Austria).

Induction (dormant) period

After the pre-induction period of fast hydration. The CAH-crystals build a barrier between the solution and the non-reacted C_3A and the hydration rate slows down significantly for one or two hours (in case of dry-mix shotcrete). The liberation of heat energy decreases significantly at the same time, cf. (Hewlett and Lea 2001, 244–45) Meanwhile, the concentration level of CH in the liquid phase reaches its maximum and declines afterwards. The SO_4^{2-} -level (if there is something left) remains constant as the fraction consumes in the formation of AFt-phases. Further information about this period, and in particular about reasons of slowing down and the later increase of hydration, can be found in (Taylor 2003, 246, 259, 260, 262)

Acceleration (post-induction) period

This stage is characterized through an accelerated hydration process, where nucleation and growth of the hydration products starts again. The C_3S hydration accelerates and CSH begins to form. In addition to that, the C_2S hydration starts. Portlandit precipitates out of the liquid phase and because of that, the concentration of Ca^{2+} declines in the liquid phase. The CAH-crystals precipitates from the C_3A -particle and the barrier between the solution and the non-hydrated C_3A is disrupted. The reaction of excessive C_3A accelerates again. cf. (Taylor 2003, 266).

Post-acceleration (deceleration) period

After reaching a maximum, the rate of hydration slows down gradually. An amount of non-reacted material declines and the hydration-rate becomes diffusion-controlled.

Additional CSH-phases are formed due to the continuing hydration process of C_3S and β - C_2S . As a result of that, the formation of calcium hydroxide declines.

Period:	Kinetics of the hydration process:	Chemical reaction:	Effects:
Pre-induction period	chemical controlled, rapid reaction	Ions get dissolved	alkaline pH-value
Induction period	slow period and nucleation	Ions get dissolved and CSH- nucleation	Begin of setting
Acceleration period	Chemical controlled rapid reaction	Begin of formation of CSH- phases	End of setting and begin of hardening
Post acceleration period	Chemical and diffusion controlled reaction	Formation of CSH- phases	influence early strength development

Table 2: Summarized stages of the hydration process

2.1.3 Heat of Hydration

As described in chapter 2.1.2, the hydration process can be divided in different periods. Each period comes with different chemical reactions and therefore with different amounts of heat release. Figure 3 shows a typical hydration curve for an ordinary Portland cement (OPC). This curve is similar to heat curves of dry-mix shotcrete. As postulated in (Hewlett and Lea 2001, 270), conducts the presence of small amounts of K^+ to a tiny initial endothermic peak right after adding mixing water. The rapid hydration of C_3S and C_3A in the pre-induction period leads to an exothermic reaction and a rather intense liberation of heat. The heat release as well as the hydration rate in the following dormant period decreases and reaches its minimum. After this induction period, the heat liberation and the hydration rate increases again, and a second exothermic peak can be observed for OPC after few days. This second increase mainly comes from the hydration of C_3S , the formation of CH and the CSH-phases. After this phase, the deceleration period occurs. The heat release decreases and reaches a low, but constant, level. In some cements, a small peak or shoulder occur at the degreasing branch of the second peak. As described in (Hewlett and Lea 2001, 270–71), this peak probably occurs because of the renewed formation of AFt. There may be another shoulder, which comes from the conversion of AFt- to AFm. In opposite to OPC, reactions of dry-mix shotcrete happens much faster. The inflection point after the dormant period appears approximately after two to ten hours. The following acceleration period emerges after about eight to eighteen hours of hydration.

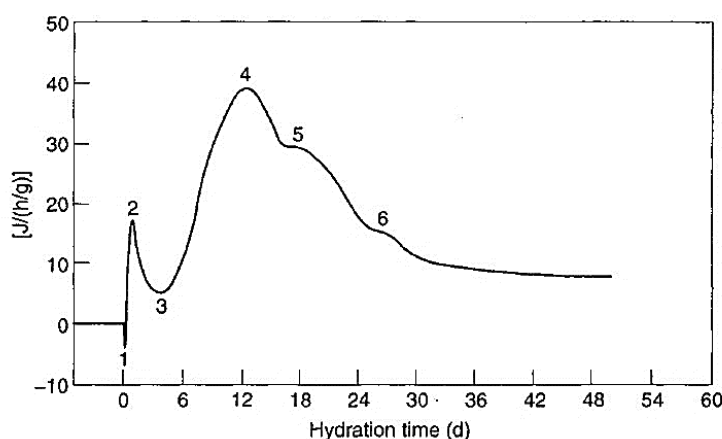


Figure 3: Example of heat of hydration curve of an OPC³

1: initial endothermic peak; 2: initial exothermic peak; 3: inflection point (dormant period ends); 4: peak of acceleration period; 5: AFt formation; 6: conversion of AFt to AFm

The general heat release results of the hydration process. It is influenced by the composition of the cement, its fineness and the surface area to volume ratio. The total heat release of the complete hydration process is approximately the sum of the heat releases of each constituent. Concerning this matter (Hewlett and Lea 2001, 271) gives enthalpy values for the hydration of each pure clinker mineral.

³ (Hewlett and Lea 2001, 270)

2.1.4 Influences on Hydration, Setting and Hardening Procedure

As described in 2.1.1, the structure, the density and within the compressive strength of solid cement paste is highly influenced by the hydration process and the water cement ratio. Up to a value of about 0.40, all added water is consumed and only gel- and air pores occur. These pores are not connected with each other. Starting from a w/c-ratio of 0.40, capillary pores appears. They are connected with each other and responsible for the water transportation through the lime. Capillary porosity lowers the compressive strength and influences the durability properties of a structure.

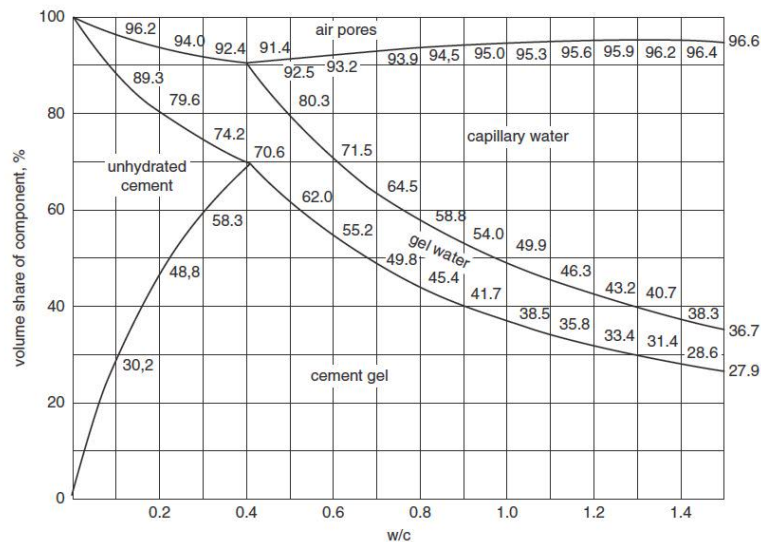


Figure 4: Pore- Distribution as a function of w/c ratio⁴

Findings in (Feldman and Cheng-yi 1985) show that a cement partially replaced with supplementary-cementitious materials, is less deformable for a given porosity than an ordinary cement paste. Feldman measured the Young's modulus, compressive strength and mercury porosity, which indicates the amount of capillary pores. The authors assumed that this might be the case because of a higher amount of CSH-phases and a lower amount of CH.

A substitution of cement with active SCMs greatly decreases the permeability to water, given that the hydration has well advanced. Results in (Marsh, Day, and Bonner 1985) show a partly substituted cement by 30% of fly ash with a permeability of $10^{-15.4}$ m/s. In comparison to that, a pure sample of Portland cement had a permeability of $10^{-11.7}$ m/s. Furthermore, similar results were found for partly substituted cement in silica fume or ground granulated blast furnace slag.

2.2 Properties of Supplementary- Cementitious Materials and Admixtures

Supplementary- Cementitious Materials (SCMs) or admixtures can be part of a dry-mix shotcrete mixture. These SCMs or admixtures affects the properties of dry-mix shotcrete in a physical or chemical manner. In general, SCMs and admixtures influence mineral growth, density, porosity and therefore the deformation behaviour of dry-mix shotcrete.

⁴ (Czernin 1980)

In a more detailed perspective two main effects emerge. First a physical filler effect occurs with addition of small amounts of inert fines ($<125\mu\text{m}$) to the blend. Therefore, fine particles occupy the space between coarser grains and less water is necessary. This leads to a low compressive strength increase. A higher amount of inert fillers reduces the compressive strength again. Findings in (Krstulović, Kamenić, and Popović 1994) showed a linear decrease of compressive strength with increasing filler proportions. Second, additional reactive fines lead to an increase of strength. This effect enhances with smaller particles and is attributable to a greater reaction surface area, cf. (Reschke, Siebel, and Thielen 1999).

2.2.1 Ground Granulated Blast Furnace Slag

Ground granulated blast furnace slag (GGBFS) is a latent-hydraulic side product in the production of pig iron. It originates from a rapid down cooling process of molten blast furnace slag through water or air. Only the fast down cooling process generates C_2S in a beta-modification, which is necessary for a hydraulic reaction, cf. (Belie, Soutsos, and Gruyaert 2018, 7–15).

Besides this reaction, there can be additional reactions for example with sulphates of cement. The additional CSH- phase causes less capillary pores and the amount of gel pores increases. As a result, the amount of free CH decreases. See also (Benedix 2015) for further information.

2.2.2 Metakaolin

Metakaolin (MK) ($\text{Al}_2\text{Si}_2\text{O}_7$) is a clay mineral, which is dehydrated by around 600 to 900°C. It reacts with CH pozzolanic to CSH-phases and strätlingite (Belie, Soutsos, and Gruyaert 2018, 191–93). The survey of (Antoni et al. 2012) showed that a coupled substitution of OPC with MK and limestone yields better mechanical properties and a tougher structure. Moreover, the study showed a decline of CH if MK and limestone is present. Findings in (El-Diadamony et al. 2016) showed equal results, whereas a substitution of cement with MK up to 20 percent leads to an increase in compressive strength in comparison to pure cement.

In addition to these previous findings, recent investigations at the Graz University of Technology showed, a reduced leaching potential of dry-mix shotcrete mixtures in presence of MK, cf. (Thumann and Röck 2017). On the contrary, the reduction of the amount of open porosity through a substitution of dry-mix shotcrete with MK could not be determined. Further findings of OPC and MK in (Frias and Cabrera 2000), confirmed these results and showed no significant difference of OPC and OPC in combination with MK in porosity during the first seven days.

2.2.3 Calcium Aluminate Cement

Calcium aluminate cement (CAC) is a non-Portland cement, which is used in this work in a mixed binder system mostly in combination with cement including calcium sulphate. The addition of CAC to Portland cement can possibly lead to a very rapid setting. This behaviour is caused by the CAC, which reacts with the calcium sulphate. This reaction disturbs the normal set control process of OPC and calcium sulphate. The needed amount of CAC depends on the type of calcium sulphate, cf. (Engineering Information, Inc 2003, 66–88). In general, CAC consists of a combination of CaO , SiO_2 and Al_2O_3 . The composition is quite distinct in comparison to Portland cement, as it can be seen in subsequent Figure 5.

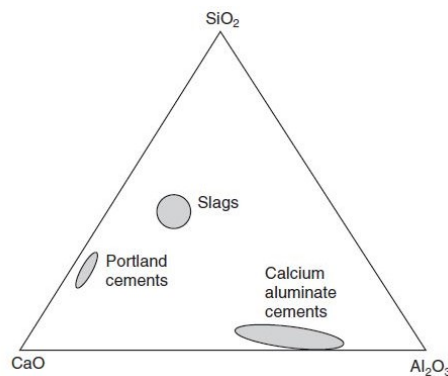


Figure 5: Composition range of CAC compared with OPC⁵

The physical hydration process of OPC and CAC is quite the same. In both reactions of the anhydrous binders with water, hydrate phases occur. However, the chemical reactions highly differ from each other. The CAC- ions dissolve in water and give a solution where different types of hydrates occur. Following equation (13) shows a typical reaction at temperatures up to 65°C, cf. (Engineering Information, Inc 2003, 69–70).



In opposite of the reaction of OPC (which is described in 2.1.1), the reaction of CAC with water only slows due to one of the reacting agents is used up or there is a lack of space for the formation of hydrates. This behaviour is illustrated in following Figure 6. This reaction manner leads to a very swift hardening and compressive strengths of more than 40 MPa at 24 hours. On the other hand, this short and intense reaction tends to result in a relatively short time where the heat of hydration evolves, cf. (Engineering Information, Inc 2003, 75–77).

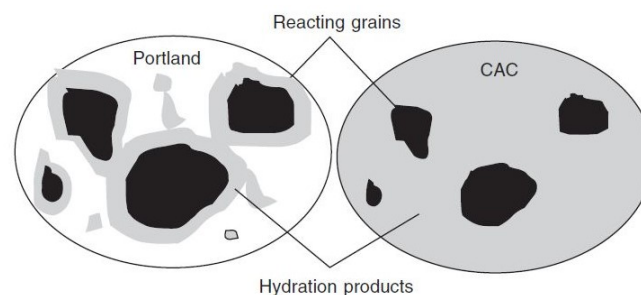


Figure 6: Reaction of OPC with H (left) in comparison with CAC with H (right)⁶

2.2.4 Limestone Powder

The limestone powder (CaCO_3) serves as a filler physically in a first glance. This leads to a denser package of cement- and limestone-grains in a paste. On a closer consideration, the limestone powder acts through a chemical reaction either, which influences the formations of AFt and AFm-phases, cf. (Matschei, Lothenbach, and Glasser 2007). The presence of fine limestone produces monocarbonate ($\text{C}_3\text{ACaCO}_3 \cdot 11\text{H}_2\text{O}$) also known as **AFmc**. It should be mentioned that the formation of this AFmc was

⁵ (Engineering Information, Inc 2003)

⁶ (Engineering Information, Inc 2003)

first detected at 7-127 days of hydration, cf. (Taylor 2003, 302–3). Beyond that, finding in (Briendl et al. 2018) showed a positive effect of ultrafine limestone powders on the early strength of wet-mix shotcrete. This effect increases with a rising particle surface area.

2.2.5 Aggregate

Aggregates in the sphere of concrete are commonly used as a filler. The amount of aggregates reduces the amount of cement in concrete. Depending on the density of the aggregate, it builds a structure, which is able to transfer a load from one grain to another grain in the hardened concrete. The compressive strength of common aggregate is much higher in comparison to an OPC- paste. An ordinary concrete collapses under compressive strength by occurring cracks, starting at the transition zone between the OPC- paste and the aggregate surface. A well-bonded connection is necessary for a high load-bearing capacity. Therefore, shape, density and surface character of single grains influence the whole system of dry-mix shotcrete significantly. Apart from these facts, the shape of single grains has a large influence on the rheological behaviour and on the necessary compressive energy.

2.3 Calorimetry

Calorimetry is a method to measure thermal energy from chemical or physical processes regardless of whether these processes are exothermic or endothermic reactions. Therefore, energy, which is the heat flow of a process, is determined by a calorimeter. Depending on the leading issue, there is a wide range of different types of calorimeters, which operate differently. In the current study, an isothermal calorimeter was used. The following subchapter describes this type of calorimeter and its functional principles in detail.

2.3.1 Basics of Thermodynamic Reactions

Chemical changes are connected with energy changes, mostly in a way of liberation or absorptions of heat energy. This process depends on available base material concentrations. Heat energy, which is liberated or absorbed through a chemical reaction, is denoted as reaction enthalpy ΔH_R . It is the difference of heat energy of a final to an initial state. A positive ΔH_R describes an endothermic and a negative ΔH_R describes an exothermic reaction. In case of an endothermic reaction, heat has to be absorbed from the surrounding. An exothermic reaction, on the other side, liberates heat at the surrounding, cf. (Benedix 2015, 81–86)

The first law of thermodynamics states that, the energy exchanges of a closed system, which comes from work **W** or heat energy **Q**, with its surrounding, is equal to changes of the inner energy **ΔU** of the system.

$$\Delta U = Q + W \quad (14)$$

The inner energy ΔU consists of:

- kinetic energy
- energy from molecular interchanges
- energy of chemical bonds
- atomic energy and its electrons

The impacts of volume changes, which are frequent in gases, are not as important for liquid and solid phases. They can be ignored for the objective work. For such simplification, it is true that the inner energy **ΔU** corresponds to the reaction enthalpy **ΔH**. Moreover, under such conditions, the reaction enthalpy can be determined by a calorimeter.

2.3.2 Isothermal Calorimetry

An isothermal calorimeter, as shown Figure 7, consists of six main parts. These are a body with a constant temperature within, a heat sink, which keeps the temperature stable, a channel for a sample, a heat flow sensor for the sample, a channel for a reference and a reference sensor.

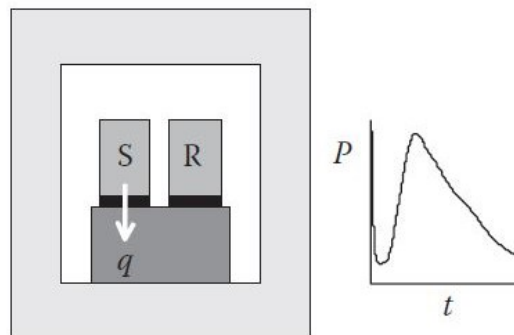


Figure 7: Schematic illustration of an isothermal calorimeter⁷

The chemical reaction of a binder in combination with additives with water is basically an exothermic reaction. Heat energy is released. The temperature in the isothermal calorimeter operates on a constant level. The generated heat is going to be compensated, and the necessary energy is recorded. This energy is equivalent to the emitted energy from the hydration process. However, the amount of heat, which is generated through hydration, is influenced by two main parameters. These influencing factors are the water- cement ratio and the temperature of the sample. The early hydration kinetics increase with a decreasing w/c-ratio, which in all probability comes from a higher concentration of alkali ions in the pore solution. In general, investigations on dry-mix shotcrete with an isothermal calorimeter are influenced mainly by following properties. These are:

- Water- to- cement ratio
- Fineness of powder
- Surrounding and precursor temperature
- Sulphate content
- Organics/admixtures
- Mineralogy

The w/c- ratio influences the heat flow of a sample. On one hand, the heat peak occurs earlier in time and it is higher with a decreased w/c – ratio. This may be due to a higher concentration of alkali ions in the initial pore solution. (Danielson 1962) On the other hand, the long- term hydration rate and the cumulative heat flow (after a period for example 24 hours) is reduced, cf. (Bentz, Peltz, and Winpigler 2009).

The fineness of powder, especially the fineness of the cement grains influences the rate of realised energy (temperature). Finer cement releases more energy than coarser grained cement, and this leads to a higher temperature, cf. (Bentz, Sant, and Weiss 2008).

Another important factor in terms of hydration and heat release is the temperature of the sample, its raw materials and it is surrounding environmental. Findings in (Kim, Moon, and Eo 1998) have shown, that, comparing to an ambient temperature of 20°C, the early strength development raises with a higher

⁷ (Scrivener, Snellings, and Lothenbach 2016, 39)

and declines with a lower temperature at the beginning of the hydration process. However, this temperature effect decreases by time and has just a little influence on the later-age strength.

2.4 X-ray Diffraction (XRD)

X-rays are electromagnetic waves with a wavelength ranging from 10^{-8} to 10^{-13} meters. They occur whenever charged particles (ions or electrons) hit a material and get stopped.

Many products, which occur during the hydration process, have a crystalline structure. Atoms, ions or molecules of minerals are regularly ordered in an abstract, representational crystal lattice. The smallest periodic repeating unit in a crystal lattice, which shows the full properties of a crystal structures, is a unit cell. This unit cell or parallelepiped is characterised by the parameters a , b , c , α , β , γ . A basic example is shown in Figure 8. The parameters a , b and c represent the x -, y -, and z -axis of coordinates in a right-handed trihedron. The angle between b and c is named α , the angle between a and c is named β and the angle between a and b is named γ . a , b , and c are vectors with their starting point at the point of origin, where from, they spread out in the three dimensions. These three vectors build in combination with the three angles α , β and γ (90° or 120°) a suitable initial lattice for a unit cell and describe the geometry of mineral.

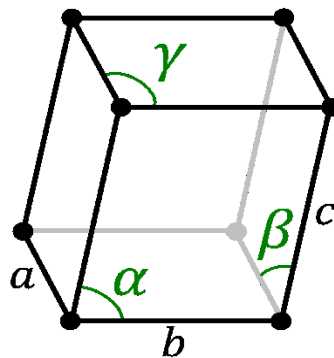


Figure 8: Basic example of a Bravais lattice⁸

Planes in such a three-dimensional lattice intersects with two or three axis of the defined coordinate system. The vectors a , b and c describe these intersection points, if they are multiplied with integer numbers m , n and p . This integer numbers are called *Weißsche indices*. However, for crystal analysis, the *Miller indices* h , k and l are more commonly used. These are the reciprocal values of the *Weißschen indices* multiplied by the least common multiple (lcm). These indices are integers, which are the smallest axis intercepts whom describe the orientation of a plane.

The distance of two coexisting planes is described by the vector d_{hkl} , and it is drawn from the origin of the unit cell to intersect the plane (hkl) at an angle of 90° cf. (Krischner and Koppelhuber-Bitschnau 1994, 67–69).

The wavelength of x - rays are in the same scale as interatomic distances. Thus, if an x - ray strikes an electron in an inner shell of an atom, the electron gets stimulated and it oscillates in the same wavelength as the x - ray wave. Because of that, the electron become a source for new rays. As it is shown in Figure 9, two beams of parallel x - ray waves with a wavelength of λ have different distances, if they strikes different lattice planes. This constructive interference yields *Bragg's law* of diffraction as shown in equation (15). This law relates the diffraction angle 2θ and the vector d_{hkl} .

⁸ URL: <https://de.wikipedia.org/wiki/Datei:Triclinic.svg#/media/File:Triclinic.svg> [15.10.2018]

$$n * \lambda = 2 * d_{hkl} * \sin \theta \quad (15)$$

As it is shown in Figure 9, the interference is two times $d * \sin(\theta)$, with d as the distance between two lattice planes and θ as the angle of incidence defined as the angle between the incoming beam and the plane. The order n is an integer number, and it gives the number of planes, which are passed.

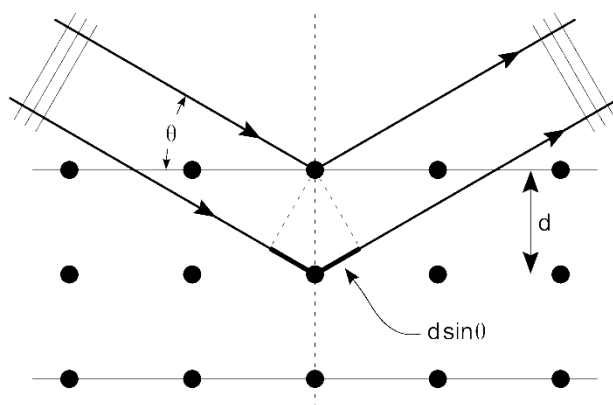


Figure 9: Bragg diffraction from a cubic crystal lattice⁹

In general, wavelength and geometry are known, whereas the plane distance is unknown. Equation (15) has to be converted and rewritten in the form of (16). The equation (16) in combination with equation (17), which is only correct in case of a cubic lattice, leads to (18). a_i represents the lattice constant in a unit cell. In a further step, the mineral can be identified in combination with a database where a_i is listed for each mineral.

$$\frac{n * \lambda}{2 * \sin \theta} = d_{hkl} \quad (16)$$

$$\frac{a_i}{\sqrt{h_i^2 * k_i^2 * l_i^2}} = d_{hkl} \quad (17)$$

$$\frac{n * \lambda \sqrt{h_i^2 * k_i^2 * l_i^2}}{2 * \sin \theta} = a_i \quad (18)$$

2.4.1 Data Analyses

XRD-observations are collections of diffraction patterns of planes of crystal lattices. The following Figure 10 shows an example of XRD-analyses. Each diffraction peak is attributed to the scattering from a specific set of planes. The Miller indices (hkl) identifies the different types of atomic planes and within the structure of the sample.

Diffraction patterns are characterised by:

- Peak position
- Peak widths
- Peak intensities

⁹ URL.: https://commons.wikimedia.org/wiki/File:Bragg_XRD.svg [29.08.2018]

3 Experimental Arrangements

The beginning of the objective work was a full-scale test (FST) of dry-mix shotcrete in Wietersdorf. A series of different blends was tested under realistic conditions. The most promising mixtures got scrutinised. These further investigations took place in a laboratory and consisted of compressive strength tests, isothermal calorimetric investigations and in-situ XRD analysis. The following chapter shows experimental assemblies and test implementations of the examined mixtures.

Sample No.:	Compressive & Bending Tensile Strength:					Calorimetry:	XRD:
	1h	3h	6h	24h	28d	0-24h	≈0-24h
W2-03-01	--	--	X	X	X	X	--
W2-03-02	--	--	X	X	X	X	--
W2-04-01	--	--	X	X	X	X	--
W2-04-02	--	--	X	X	X	X	--
W2-10-01	--	--	X	X	X	X	--
W2-10-02	--	--	X	X	X	X	--
W2-11-01	--	--	X	X	X	X	--
W2-11-02	--	--	X	X	X	X	--
W2-12-01	--	--	X	X	X	X	--
W2-12-02	--	--	X	X	X	X	--
W2-13-01	--	--	X	X	X	X	--
W2-13-02	--	--	X	X	X	X	--
W2-13-03	--	--	X	X	X	X	--
W2-14-01	--	--	X	X	X	X	--
W2-14-02	--	--	X	X	X	X	--
W2-14-03	--	--	X	X	X	X	--
REF-1-01	--	--	X	X	X	X	X
REF-1-02	--	--	X	X	X	X	--
REF-1-03	X	X	--	--	--	--	--
REF-1-04	X	X	--	--	--	--	--
REF-2-01	--	--	X	X	X	X	X
REF-2-02	--	--	X	X	X	X	--
REF-2-03	X	X	--	--	--	--	--
REF-2-04	X	X	--	--	--	--	--

X: examined --: not examined

Table 3: Overview of the experimental programme

3.1 Raw Materials

The following Table 4 to Table 7 represents and describes the base material of this work.

Description	Shortcut:	Density [g/cm ³]	d ₅₀ [μm]	BET [m ² /g]	Blaine [m ² /g] approxi- mate value
Binder:					
CEM I 52.5 N – SRO C ₃ A-free	CEM-SRO	3,26	8,0	0,96	4193
“Spritz-Bindemittel DT”	SPBM-2	3,14	8,0	1,03	4002
Meso- filler (MEF):					
Ground granulated blast fur-	MEF-	2,91	8,6	0,91	3919
CaAlCem PP	CAC-222	3,21	13,9	--	--
CaAlCem SC1	CAC-SC1	3,00		--	--
High- hydraulic lime	NHL-5OT	2,75		--	--
Micro- filler (MIF):					
Limestone powder “Extra GU”	MIF-CAL-EGU	2,72	1,2	5,65	*(23594)
Metakaolin SF	MIF-MET-SF	2,47	2,1	8,59	*(28273)
Aggregate:					
Dolomite “Eberstein premix”	GK-DOL-0/8	2,84		--	--
Admixtures:					
Accelerators (powder)	EB S49 AF			--	--
Rebound- reducer 1	RP1 NAF				
Rebound- reducer 3	RP3 AMI				
Rebound- reducer 4	RP4 BENTO				

Table 4: List of raw materials that was used in Wietersdorf 2018

Description:	Ser. No.:	Shortcut:	Density [g/cm ³]	d ₅₀ [μm]	BET [m ² /g]
Cement:					
CEM I 52.5 N – SRO C ₃ A- free	395/16	CEM-SRO	3.26	7.97	0.96
Spritz-Bindemittel DT	--	SPBM-2	3.14	7.99	1.03
Meso- filler:					
Ground granulated blast furnace	387/16	MEF-HÜS_4500	2.91	8.58	0.91
CaAlCem PP	420/16	CAC-222	3.21		13.86
CaAlCem SC1		CAC-SC1	3.00		
Micro- filler:					
Kalkmehl Extra GU	342/16	MIF-CAL-EGU	2.72	1.16	5.65
Metakaolin SF	389/16	MIF-MET-SF	2.47	2.12	8.59
Aggregate:					
Holler 0/4	--	Holler 0/4	2,60-2,66	--	--
Admixtures:					
Superplasticizer: Sika® Vis- coCrete® -20 HE	--	FM 554_113/18	--	--	--

Table 5: Base material for laboratory experiments

Sample No.:	395-297/16	388-283/16	342-227/16	389-287/16
Shortcut:	CEM I SRO	SPBM-2	MIF-CAL-EGU	MIF-MET-SF
Material:	CEM I SRO	SB-Durocem	Limestone powder	Metakaolin
Lol	4.0	1.8	42.6	2.0
Na ₂ O	0.4	0.7	0.1	<0.1
MgO	1.2	2.0	1.5	<0.1
Al ₂ O ₃	2.9	6.1	0.1	44.7
SiO ₂	20.2	20.6	1.1	50.7
P ₂ O ₅	<0.1	0.3	<0.1	<0.1
SO ₃	2.3	1.2	<0.1	<0.1
*S	--	--	--	--
K ₂ O	0.4	0.7	<0.1	<0.1
CaO	64.0	63.4	54.6	<0.1
TiO ₂	0.2	0.3	<0.1	1.7
MnO	<0.1	0.1	<0.1	<0.1
Fe ₂ O ₃	4.3	2.8	0.1	0.6
Σ	99.8	100.0	100.0	99.7

Table 6: Chemical components of base materials

Sample No.:	395-297/16	388-283/16	342-227/16	389-287/16
Shortcut:	CEM I SRO	SPBM-2	MIF-CAL-EGU	MIF-MET-SF
Material:	CEM I SRO	SBA ^a	Limestone powder	Metakaolin
Calcit	9.4	0.5	95.5	--
Dolomit	--	0.8	3.9	--
Anhydrit	3.3	--	--	--
Basanite	1.3	1.2	--	--
Alit C3S M3	56.1	59.1	--	--
Belit b-C2S	13.4	13.8	--	--
Aluminate C3Ac	0.7	7.6	--	--
Aluminate C3Ao	1.3	3.7	--	--
Ferrit C4AF	12.8	8.2	--	--
Aphtitalit	0.9	0.7	--	--
Arkanit	--	0.6	--	--
Portlandit	0.7	2.5	--	--
Free lime CaO	--	0.3	--	--
Periclas	--	1.0	--	--
Magnetit	--	--	--	--
Anatas	--	--	--	1.7
Quarz	--	--	0.6	0.5
Cristobalit	--	--	--	--
K- Feldspat	--	--	--	0.5
Albit/ Plagioclas	--	--	--	--
Mullit	--	--	--	--
Gehlenit	--	--	--	--
Muskovit	--	--	--	--
Kaolinit	--	--	--	2.9
Amorph	--	--	--	94.4
Σ	99.9	100.0	100.0	100.0

^a **Spryable Binding Agent**

Table 7: Mineralogical components of base materials

3.2 Full-Scale Test

The full-scale dry-mix shotcrete test took place in Wietersdorf (Carinthia, Austria) at a cement plant in the time from 12th to the 16th of March 2018. One of the assignments was to investigate the mixtures of ordinary Portland cement (OPC) with some other supplementary cementitious (SCMs) and admixtures in terms of strength development. Each mixture was weighted and mixed on site. The dry mixture was pumped through a hose to the nozzle, whereas water was added in a certain amount by a professional nozzleman. The shotcrete was sprayed towards a wall where boxes were placed in advance. These boxes, filled with hardened shotcrete was investigated afterwards through different tests. This chapter 3.2 and its subchapters gives a brief overview of the findings in terms of strength development. Detailed information are evident in the report (Juhart J. et al. 2018).

3.2.1 Aggregates for the Dry-mix shotcrete of the Full-Scale Test

The shotcrete at the full-scale test was made with the aggregate "Eberstein 0/8". This is aggregate consisting of dolomite with a maximum grain size of 8 mm. The following Figure 11 shows the grain-size-curve of the used aggregate. In addition to that, Figure 11 shows the ideal maximum-density-curve and the upper and lower grain-size borders, which are recommended by the "Österreichische Bautechnik Vereinigung" (ÖBV), a society of building techniques in Austria.

According to that illustration, it can be seen that the applied aggregate is in line with the idealistic maximum density curve at the upper part of the diagram. However, smaller grain sizes are underrepresented in comparison with the optimal grain-size distribution, which can be calculated with equation (19).

$$A_i = \left(\frac{d_i}{D_{max}}\right)^{0.5} \tag{19}$$

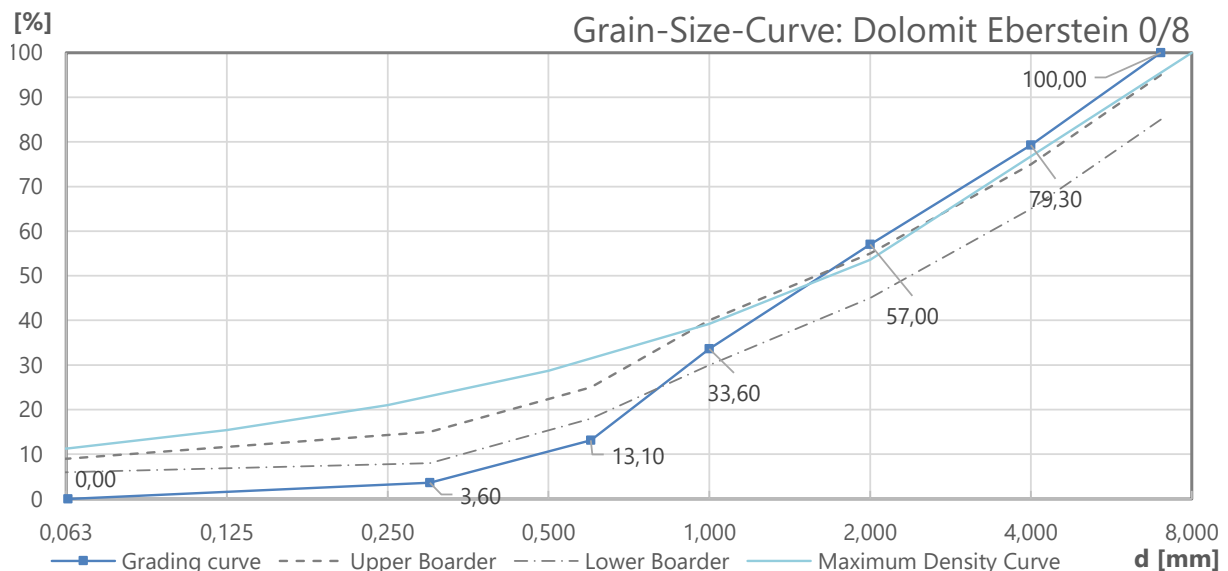


Figure 11: Grain-size-curve of the aggregate, which was used at the full-scale test

3.2.2 Recipes

The following Table 8 shows all mixtures from the full-scale test in Wietersdorf. The greyish rows were selected for further investigations in the laboratory. Moreover, the dark grey coloured row was modified in the laboratory.

Sample No.	W/B-ratio	SPBM2	CEM SR0: Cement CEM I 52.5 N SR0 C ₃ A-free	CAC 222: calcium aluminat cement 222	CAC SC1: calcium aluminat cement SC1	MEF-HÜS-4500	MIF-CAL-EGU	MIF-MET-SF	Additives
W1	0,60	80%				20%			
W2	0,47		90%				7%		3%EB ^a
W3	0,49		90%		10%				
W4	0,47		70%		10%	15%	5%		
W1- WH	0,49	80%				20%			
W5	0,51	80%				19.3%			0.7% RPM ^b
W6	0,47	80%				19.85%			0.14% RPM ^b
W7	0,60	80%				20%			
W8	0,50	80%				10%			
(W9)	--	70%				20%	10 %		
W10	0,41	70%		10%		20%			
W11	0,45	70%		5%		15%	5%	5%	
W12	0,50	75%				15%	5%	5%	
W13	0,38	70%				20%	10 %		1.2%FM ^c
W14	0,46	50%		7%	3%	30%	5%	5%	0.8% FM ^c 0.14% RPM ^b

^a accelerator ^b rebound reducer ^c plasticizer

Table 8: Blends from the full-scale test in Wietersdorf

3.2.3 Compressive Strength Results

The very early CS-test was made soon after spraying during the first 24 hours of hydration. Therefore, a bolt was pushed with a powder actuated nail gun into the young but solid shotcrete. The ratio of penetration depth and extraction force occasioned in combination with the conversion curves from the manufacturer to the approximate CS-value. This method is a standardised procedure. Detailed information about the exact implementation can be seen in (ÖNORM EN 14488-2 2006).

In addition to that, drill cores, 100 millimetres in diameter, was taken from the sprayed shotcrete surface. These drill cores got labelled and stored under water and was brought to the laboratory at the Graz University of Technology. Following this, the cores got stored under water until the twenty-eighths day of hydration. Then they were tested for CS.



Figure 12: Experimental arrangement:
 1: Powder actuated nail gun; 2: Nail; 3: Nail with a washer and an unscrewed head; 4: removing device¹¹

The following table indicates the results from the CS-test after ten minutes, six hours and 28 days. The greyish coloured lines are those who are reproduced in the laboratory.

Sample No.:	Shortcut:	Early strength*		Strength
		10 min. [N/mm ²]	6h [N/mm ²]	28d [N/mm ²]
W1	Ref SPBM80	1,0	1,8	46,7
W1 WH	WH Ref SPBM80-HÜS20	1,2	3,0	60,9
W2	Ref SR090-CAL7-EB3	0,05	4,0	66,3
W3	SR090-CAC(SC1)10	1,1	4,5	66,3
W4	SR070-CAC(SC1)10-HÜS15-CAL5	2,1	8,0	78,2
W5	SPBM80-HÜS19-RPM1	1,2	3,0	60,2
W6	SPBM80-HÜS20-RPM3	1,1	4,5	57,5
W7	SPBM80-HÜS20-RPM4	0,7	1,9	43,1
W8	SPBM80-HÜS10-NHL10	1,0	5,0	48,8
(W9)	SPM70-HÜS20-CAL10 FM	--	--	--
W10	SBM70-CAC(222)10-HÜS20	2,0	8,8	60,3
W11	SBM70-CAC(222)5-HÜS15-CAL5-MET5	1,0	2,5	57,5
W12	SPM75-HÜS15_CAL5-MET5	1,0	3,0	69,8
W13	SPM70-HÜS20_CAL10 FM	1,0	5,1	74,8
W14	SPBM50-CAC(222)7-CAC(SC1)3-HÜS30-CAL-MET5-RPM3-FM	0,9	4,5	63,2

*estimated

Table 9: Compressive strength results from the full- scale test

¹¹ (Juhart J. et al. 2018, 11)

3.3 Laboratory Tests

This chapter describes the experimental arrangements in the laboratory, which tried to verify the results of the full-scale test in Wietersdorf. The investigations contained bending tensile strength tests, compressive- strength tests as well as calorimetry- and XRD-analyses. The following subchapter gives a description of these tests.

3.3.1 Raw Material and Recipes

The following **Fehler! Verweisquelle konnte nicht gefunden werden.** represents the list of materials with their properties and shortcuts followed by Table 10 and Figure 13, which presents the selected mixtures from the full-scale test. It should be mentioned that mixture W2-11b is slightly different to W2-11. It contains five percent of CAC SC1 instead of five percent CAL EGU.

Sample No.	W/B-ratio	SPBM2	Durocem T	CEM SR0: Cement CEM I 52.5 N SRO C ₃ A-free	CAC PP 222: calcium aluminate cement PP 222	CAC SC1: calcium aluminate cement SC1	MEF-HÜS-4500	MIF-CAL-EGU	MIF-MET-SF	Additives
W3	0.50			90%		10%				
W4	0.50			70%		10%	15%	5%		
W10	0.50		70%		10%		20%			
W11 b	0.50		70%		5%	5%	15%		5%	
W12	0.50		75%				15%	5%	5%	
W13	0.38		70%				20%	10%		1.2% FM ^a
W14	0.50		50%		7%	3%	30%	5%	5%	0.8% FM ^a
REF 1	0.50		100%							
REF 2	0.50			90%		10%				

^a FM: plasticizer

Table 10: Mixtures produced in the laboratory

Blending overview:

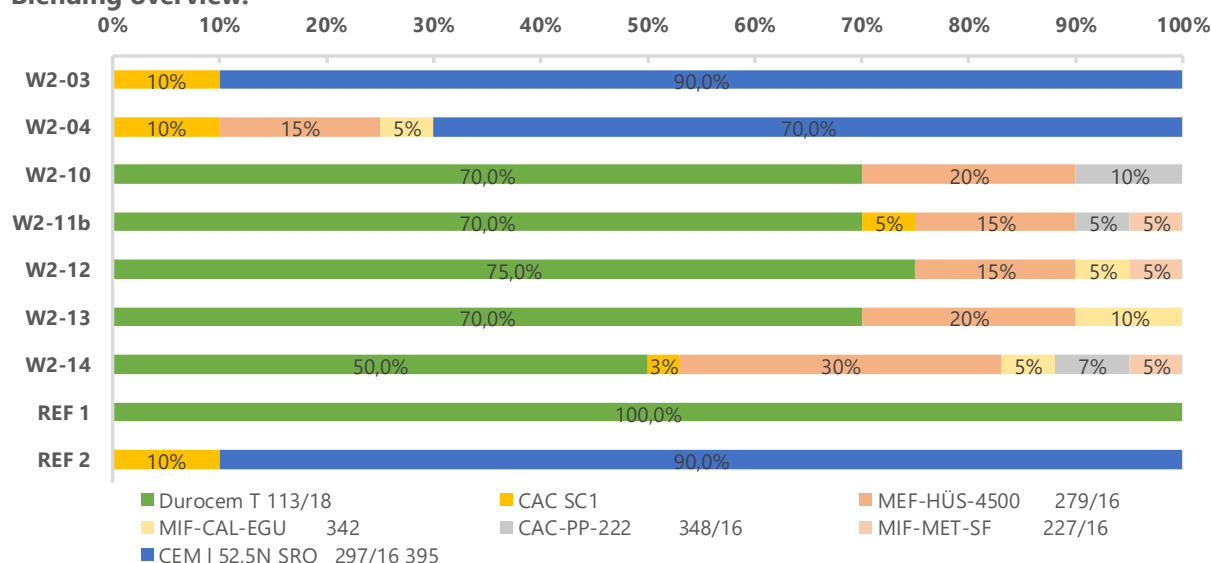


Figure 13: Mixtures with its components

3.3.2 Aggregate of Dry-mix Mortar for Laboratory Tests

The objective dry-mix shotcrete samples were made with the aggregate "Holler 0/4". This is an aggregate with a maximum grain size of 4 mm. The following Figure 14 shows the grain-size-curve of the used aggregate. In addition to that, the figure below shows the ideal maximum-density-curve, which was calculated with equation. (19). According to this illustration, it can be seen that the objective aggregate does not correspond to the optimal curve.

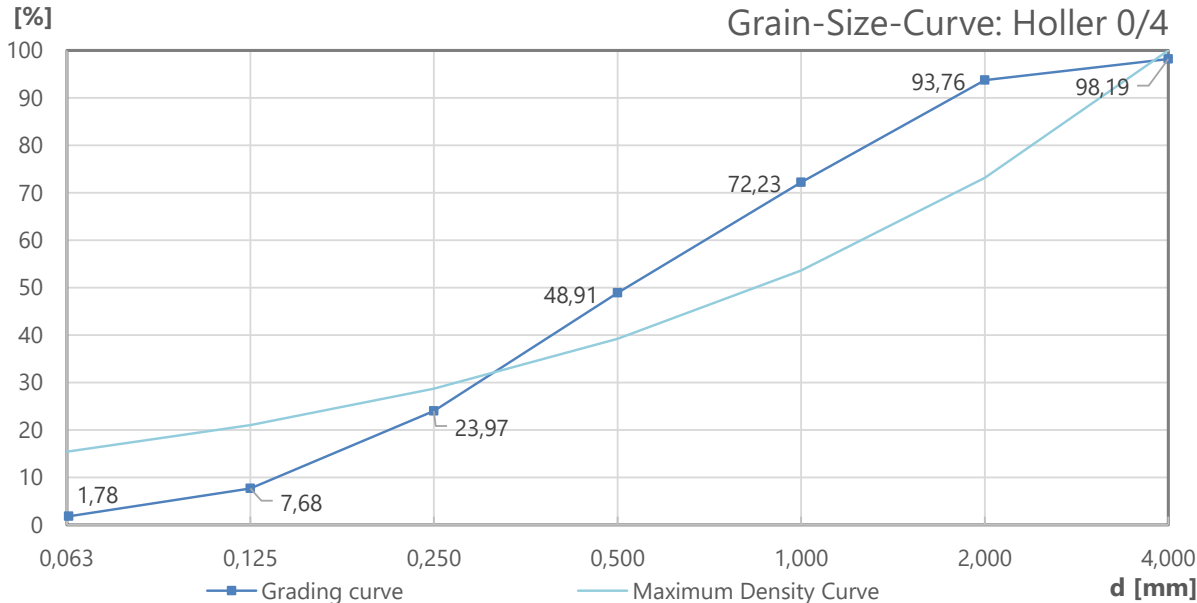


Figure 14: Grain-size-curve of used aggregate in the laboratory tests

3.3.3 Mixing Procedure

The data quality depends on a realistic manufacturing method, which is realizable by a single person. The following method was developed and tested through many trials before the actual tests has started.

Manufacturing method of test specimen W2-02 to 14:

At the beginning, the raw materials and the entire equipment needs to be prepared. Therefore, the raw materials need to be stored in the laboratory for at least 48 hour to achieve ambient temperature. An oiled formwork, which consists of three moulds for three prismatic samples (40x40x160mm), is placed on a vibrator next to a mixer. The mixing-routine starts with weighting water, aggregates, powders and if needed admixtures in appropriate quantity. Therefore, each mix consist of 600g powder (cement and other admixtures), 1200g aggregate and 300g water (for a W/B- ratio of 0.50). The different types of powder are mixed with the aggregate in a bowl to be sure that all raw materials are perfectly distributed in the dry mixture. In a next step, the entire water is filled into the mixing bowl, and the mixer is turned on with 150 rpm per minute. Then, the entire ready dry-mixed powder is added and mixed for 15 seconds with 300 turns per minute. After that, the finished mixture is filled in the prepared prismatic formwork, which vibrates for at least 30 seconds to get the dry- mix shotcrete compacted. Lastly, covers an oiled glass plate the formwork, and the formwork is stored by 100% humidity until the first bending tension- and compressive strength- test starts.

3.3.4 Bending Tension- (BT) and Compressive-strength-Test (CS)

In general, the test cycles are six (± 15 min) and twenty- four hours (± 15 min) as well as twenty-eight days (± 8 h) after the first addition of mixing water (time of manufacturing), cf. (ÖNORM EN 196-1: 2016 10 15 2016). In addition to this test cycle, BT- and CS-tests were performed for the reference mixtures REF1 and REF2 after one (± 5 min) and three hours (± 5 min).

In a first step, all manufactured samples were stripped from there formwork, the overall dimensions were measured (± 0.01 mm) and the weight were determined (± 0.01 g). The obtained data (length, width, height and weight) were documented afterwards. In a second step, the bending tension and the compressive strength was tested through destructive tests according to the ÖNORM EN 196 – methods of testing cement. The BT was determined by the "ToniNORM"-machine, an instrument from "ToniTechnik", shown in Figure 16. The samples broke under pressure in two, nearly equal sized pieces. The cracking load was documented for further evaluations. Each of these two-pieces were tested afterwards, depending on there state of hydration, in a CS-testing machine. The CS-testing instrument, which was used during the first 24 hours, was the "AUTOGRAPH AG-50kNG" from "SHIMADZU" and the tests were performed with a crosshead speed of 1mm/min. Later CS-investigations were conducted with the "ToniNORM" from "ToniTechnik", which is shown in Figure 15.

Instrument:	Max. Load Capacity:	Accuracy:
SHIMADZU Autograph AG-50kNG	50 kN	within $\pm 1\%$ indicated test force
ToniTechnik ToniNorm (CS)	300 kN	quality class 1 (EN ISO 7500-1)
ToniTechnik ToniNorm (BT)	10 kN	quality class 1 (EN ISO 7500-1)

Table 11: Machine specifications



Figure 15: Compressive Strength-testing machine "ToniNORM" (300kN)

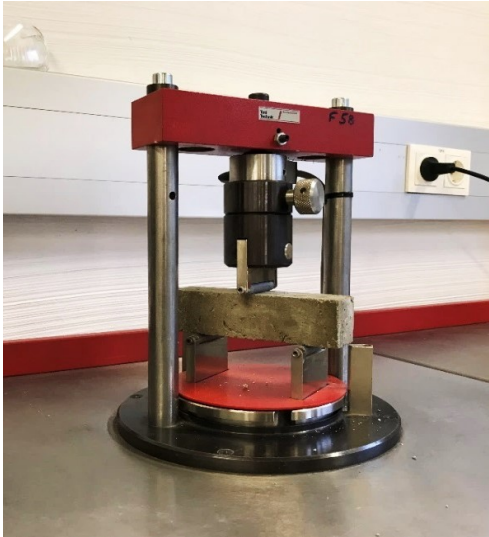


Figure 16: Bending tensional-testing machine "ToniNORM" (10kN)

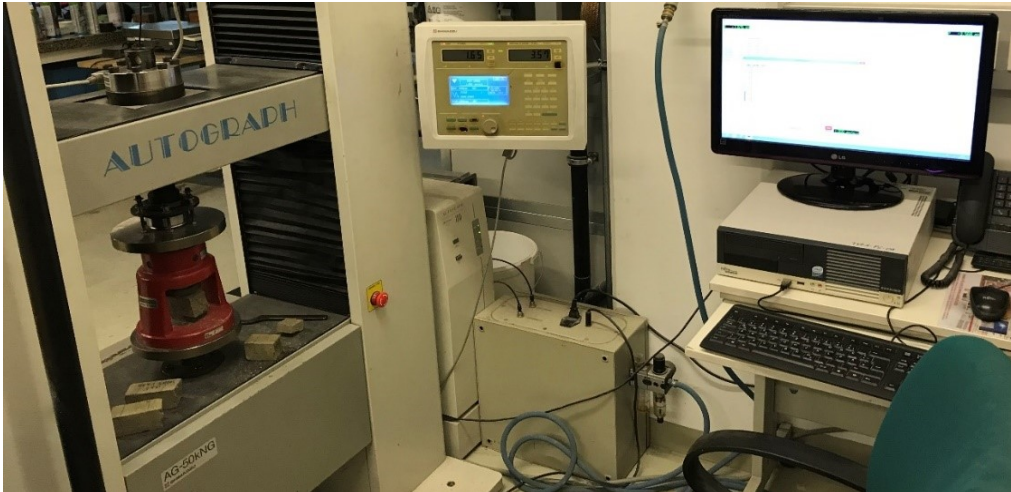


Figure 17: Compressive strength-testing machine "SHIMADZU AUTOGRAPH AG-50kNG" (50kN)

3.3.5 Calorimetry

The following paragraph describes the implementation of isothermal, calorimetric investigations with a calorimeter. The current device is the "I-Cal 4000 HPC", a calorimeter with four channels from *calmetrix*. It has an operating temperature ranging from 5°C to 70°C (+/- 0.02°C), and is calibrated on a temperature of 20°C. It measures the thermal power in Watts with a drift < 0.05μW/g/h. This calorimeter comes with the software *CalCommander*, which is able to show thermal power and heat flow in real time.

Realization of calorimetric investigations on specimens W2-02 to 14, REF 1 and REF 2:

At the beginning, all powders, aggregate and mixing water need to be prepared and stored next to the calorimeter in the laboratory for at least 48 hours to reach the ambient temperature of the calorimeter. Then, all sample cups are weighted and labelled. Next, the dry-mix blends are prepared and blended as it was described in 3.3.3. The sample cups were filled immediately with a tablespoonful of extracted mixture. Following this, the filled sample cups are rapidly set in the channels, where the energy flow is measured every 15 seconds, for at least 24 hours. In the final step, all samples were removed and weighted to get the mass of the specimen itself.



Figure 18: Calorimeter "I-Cal 4000 HPC"

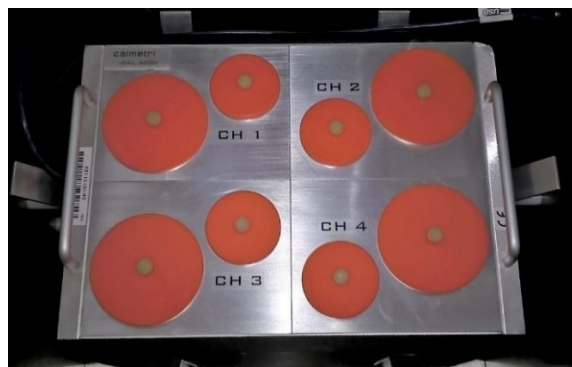


Figure 19: Inside look of isothermal test units

3.3.6 X-ray Diffraction (XRD)

The in-situ XRD-investigations with fresh dry-mix shotcrete demanded a very rapid realization to follow the hydration process for approximately 24 hours. Therefore, 90 measurements were made, whereas each observation ranged from about nine to 50° (2θ) and lasted approximately 15 minutes. This procedure expresses a compromise of data quality and the requirement of studying as many hydration steps as possible during the early stage of hydration.

However, the database for the following investigations was the American Mineralogist Crystal Structure Database (AMCSD). These XRDs-patterns were made with a copper anode. The current XRD device operates with a cobalt anode. Therefore, an angular transformation has to be made and the 2θ-angle from the database has converted to a cobalt anode with equation (20). The two variables in this equation are the wavelength of cobalt (L₁) and the wavelength of copper (L₂).

$$2\theta(Co) = 114.59156 * \sin^{-1} \left\{ \frac{L_1}{L_2} * \sin[0.00872664 * 2\theta(Cu)] \right\} \quad (20)$$

With:

$$L_1 = 1.7891$$

$$L_2 = 1.5418$$

Realization of the XRD investigations for specimen REF 1 and REF 2:

First, the pre-weighted base material, the blender, a sample holder and a piece of a "Kapton"-film need to prepare as close as possible to the diffractometer. When the preparation is done, the background of the "Kapton"-film needs to determine by using a single crystal silicon wafer. This background has to subtract from the measurements afterwards. In the main step, the mixture needs to be produced. The mixing procedure and composition is equal to the procedure of mortar-samples, cf. 3.3.3. The only distinction between the past samples for XRD-analysis and mortar samples is the additional aggregate in the mortar samples. A small amount of the mixture has to extract from the pot. The extracted material needs to be filled and coated smoothly into the sample holder as fast as possible. Then, the surface has to covered with a "Kapton" film (7.6 μ m) right afterwards to prevent the paste from drying during the in-situ experiment. In a final step, the sample holder is placed in the diffractometer to measures the sample in time steps of about 15 minutes continuously for about 24 hours in the range of 9° to 50° (two theta).

**Figure 20:** XRD chamber**Figure 21:** XRD-machine

4 Experimental Results

This chapter presents the results from the laboratory test. First, the CS-accomplishments are shown followed by the results from the calorimeter- and XRD-investigations. The detailed results can be seen in the appendix, whereas appendix A displays the properties of each sample, appendix B exhibits all stress-strain-curves from each sample and appendix C shows the heat release curves from the calorimeter.

4.1 Strength Development of Dry-mix Shotcrete

According to 3.3.4, this chapter presents the result of compressive strength tests of dry-mix shotcrete at testing intervals of six hours, 24 hours and 28 days for the samples W2-03 to W2-14. In addition to that, the samples REF-1 and REF-2 were tested even at one and three hours. For a better survey, the results of specimens with CEM I 52,5N SR0-cement and SPBM2 are marked in different colours. In the following diagrams, samples containing SR0-cement are blue, those containing SPBM2 are coloured green.

4.1.1 Compressive Strength of Series W2-03 to W2-14

As it is shown in Figure 22, mixtures W2-04 and W2-11b, have by far the greatest CS-values after six hours, whereas W2-10, W2-12 and W2-14 have relative small CS-values. The CS-results after 24 hours look differently in comparison to results than those after six hours. Sample W2-10, W2-12 and especially W2-13 made up leeway compared with to W2-04 and W2-11b. Moreover, W2-13 has the greatest CS-value after 24 hours. The results of the CS-investigations after 28 days show nearly the same CS-values for samples with SR0-cement independently from their supplies. However, samples containing SPBM2 show a stronger dependency of added SCM- and admixtures. The detailed CS-results for each test series are shown in following Table 12. The table displays the sample standard deviation (SSD) in addition to the CS-results.

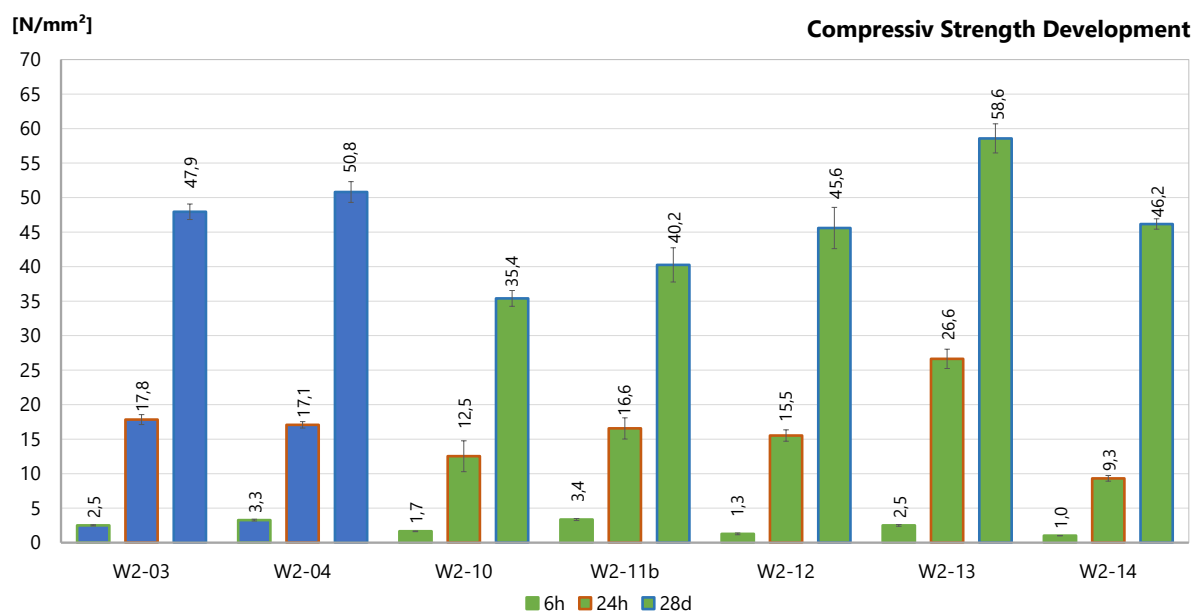


Figure 22: Results from CS-tests at 6h, 24h and 28d

Sample:	6h CS [N/mm ²]	SSD [N/mm ²]	24h CS [N/mm ²]	SSD [N/mm ²]	28d CS [N/mm ²]	SSD [N/mm ²]
W2-03	2.51	0.08	17.84	0.72	47.94	1.13
W2-04	3.27	0.13	17.08	0.47	50.81	1.51
W2-10	1.65	0.05	12.53	2.23	35.39	1.15
W2-11	3.35	0.15	16.65	1.53	40.25	2.48
W2-12	1.28	0.13	15.53	0.83	45.60	2.98
W2-13	2.50	0.13	26.65	1.40	58.58	2.11
W2-14	1.02	0.03	9.32	0.41	46.18	0.74

Table 12: CS-results of samples W2-03 to W2-14 with sample standard deviation (SSD)

4.1.2 Compressive Strength of Series REF1 and REF2

The bar chart below represents the results of mixtures REF1 and REF2. The very early CS-levels of the greenish coloured REF1 and the bluish REF2 are almost equal. The CS-values of both increases equally by time until the first 24 hours of hydration. In comparison to that, the CS-development of both mixtures differ from each other in later stages. The following illustration shows a significantly greater CS-value of REF2. The detailed CS-result for each test series is shown in Table 13. The table includes the SSD in addition to the CS-results.

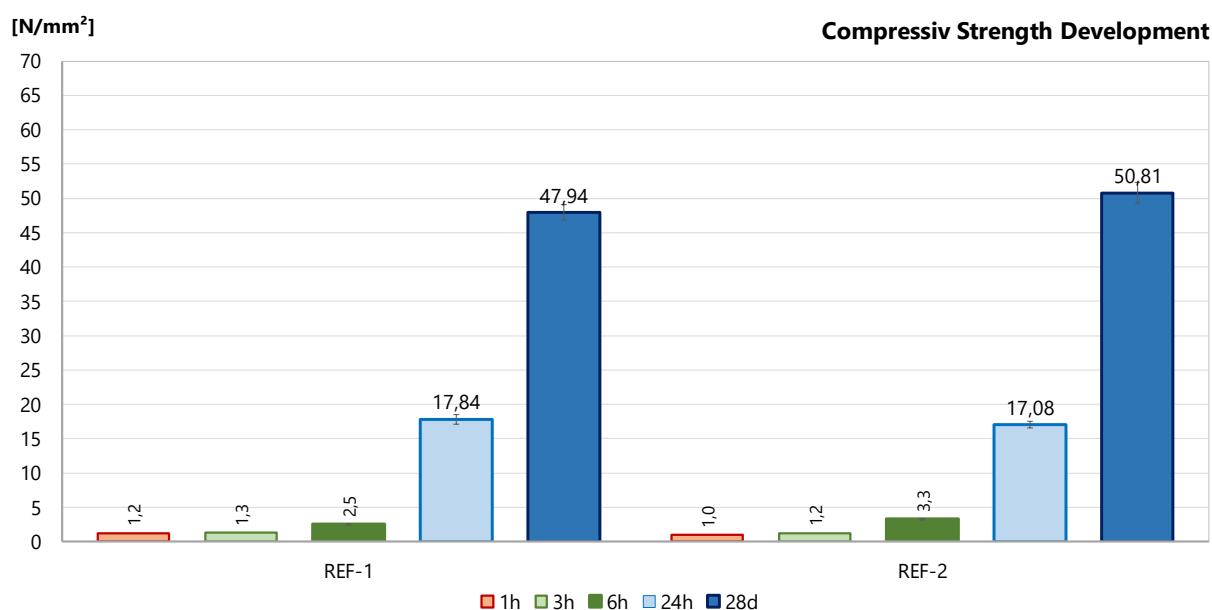


Figure 23: Results from CS-tests at 1h, 3h, 6h, 24h and 28d

Sample:	1h CS [N/mm ²]	SSD [N/mm ²]	3h CS [N/mm ²]	SSD [N/mm ²]	6h CS [N/mm ²]	SSD [N/mm ²]	24h [N/mm ²]	SSD [N/mm ²]	28d [N/mm ²]	SSD [N/mm ²]
REF 1	1,23	0.06	1.30	0.03	2.15	0.25	19.32	0.68	36.95	2.78
REF 2	0,96	0.03	1.18	0.08	2.57	0.20	19.19	0.67	51.09	4.62

Table 13: CS-results of samples REF 1 and REF 2 with SSD

4.2 Calorimetry

This chapter contains the results of thermodynamic examinations of dry-mix shotcrete. The chapter is divided into four sections. The first section presents the outcomes of the investigations on the mixtures W2-03 and W2-04, containing SRO-cement and some SCMs. The second section focusses on the results of W2-10 to 14. These samples contained SPBM2 in combination with supplies as described in 3.3.1. The third and fourth section present the results of REF-1 and REF-2. These two displays the investigations with SRO and SPBM2 more accurately. The markings P1, P2 and P2 in the figures stands for the hydration periods one, two, three and four.

Mixtures W2-03 and 04 with CEM I 52,5N SRO

Figure 24 shows the initial reaction of the hydration on the left-hand side. The right right-hand side focuses on the dormant, post-induction and deceleration period. Table 14 reflects detailed information of the stages of hydration. The mixtures W2-03 and W2-04 react equally at the initial stage. However, the acceleration period of mixture W2-03 starts a little bit early and has a higher peak at the end of this phase in comparison with W2-04. The cumulative heat progress, which is shown in Figure 25, indicates equal features. Both mixtures emit nearly the same amount of heat energy until the first nine hours. A further progress shows a 11% higher heat energy production of W2-03 in comparison to W2-04 after the first 24 hours.

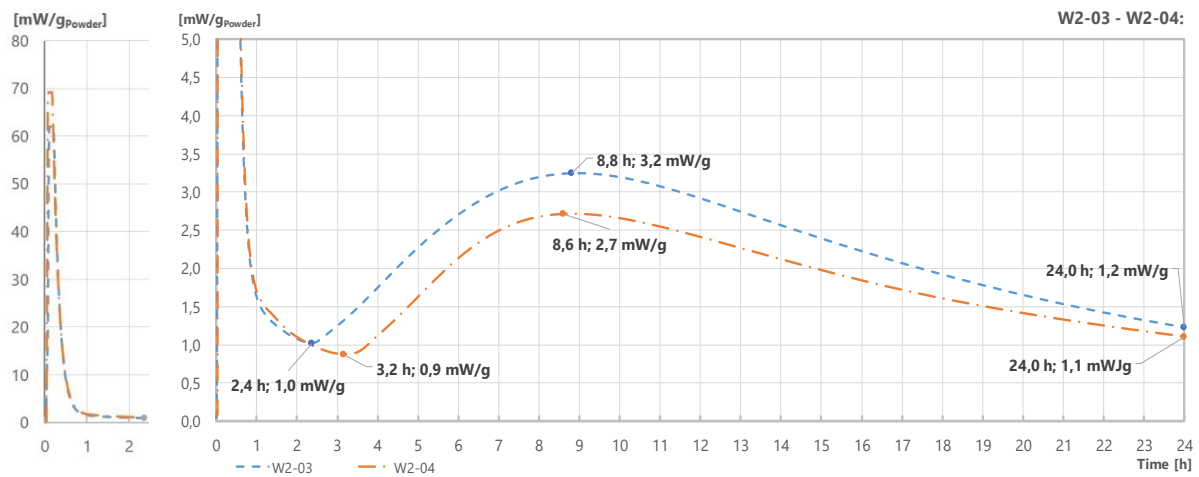


Figure 24: Heat of hydration of dry-mix shotcrete mortar with CEM I 52,5N SRO

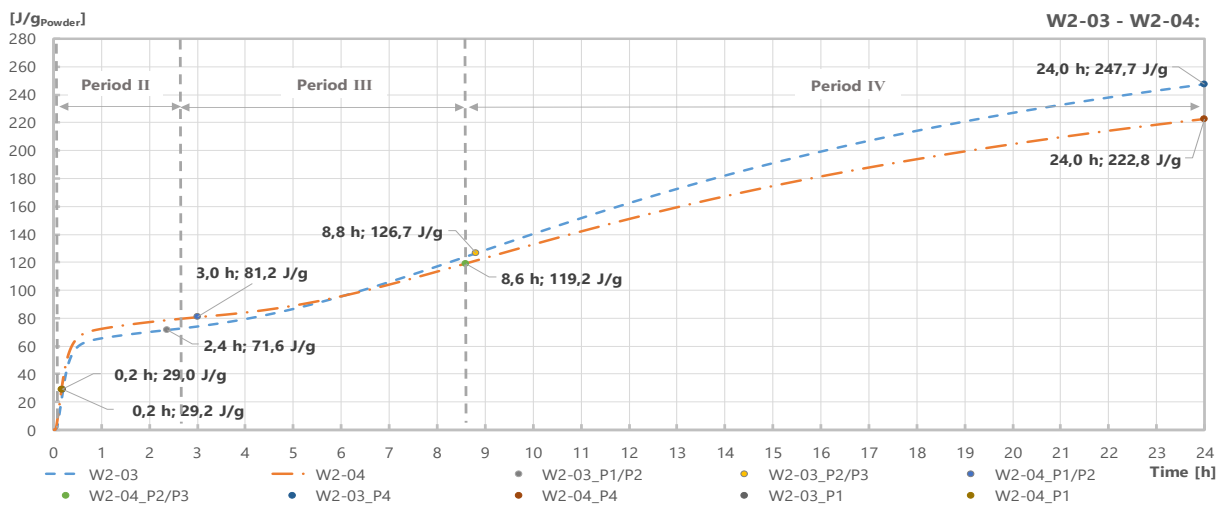


Figure 25: Cumulative heat of hydration of dry-mix shotcrete mortars with CEM I 52,5N SRO and other SCMs

Periods:	W2-03:	W2-04:	
Period I	Start [h]	0.00	0.00
	End [h]	0.20	0.17
	Δt [h]	0.20	0.17
	Power [mW/g]	62.02	69.23
	Heat Release [J/g]	29.24	28.98
Period II	Start [h]	0.20	0.17
	End [h]	2.37	3.17
	Δt [h]	2.17	3.00
	Power [mW/g]	1.02	0.87
	Heat Release [J/g]	71.56	81.18
Period III	Start [h]	2.37	3.17
	End [h]	8.82	8.60
	Δt [h]	6.45	5.43
	Power [mW/g]	3.24	2.71
	Heat Release [J/g]	126.66	119.21
Period IV	Start [h]	8.82	8.60
	End [h]	24.00	24.00
	Δt [h]	15.18	15.40
	Power [mW/g]	1.23	1.10
	Heat Release [J/g]	247.67	222.78

Table 14: Summary of the hydration periods of dry-mix shotcrete mortars with CEM I 52,5N SRO and SCMs

Mixtures W2-10 to W2-14 with SPBM2

The heat release in Figure 26 shows mixtures, which contain SPBM2. The highest peak can be seen at the very beginning of each reaction regardless whether which supplies were added. The detailed progress on the right hand side of Figure 26 is a cut-out and focuses on the dormant, post-induction and deceleration period. Mixtures W2-10, W2-11b and W2-14 show a short increase of the liberation of heat during the dormant period. These mixtures contain CAC-PP222, which differentiates them from all the other samples. Furthermore, the data showed that mixture W2-13 liberates the most heat energy. While mixture W2-12 exhibits the lowest heat release during the first 24 hours.

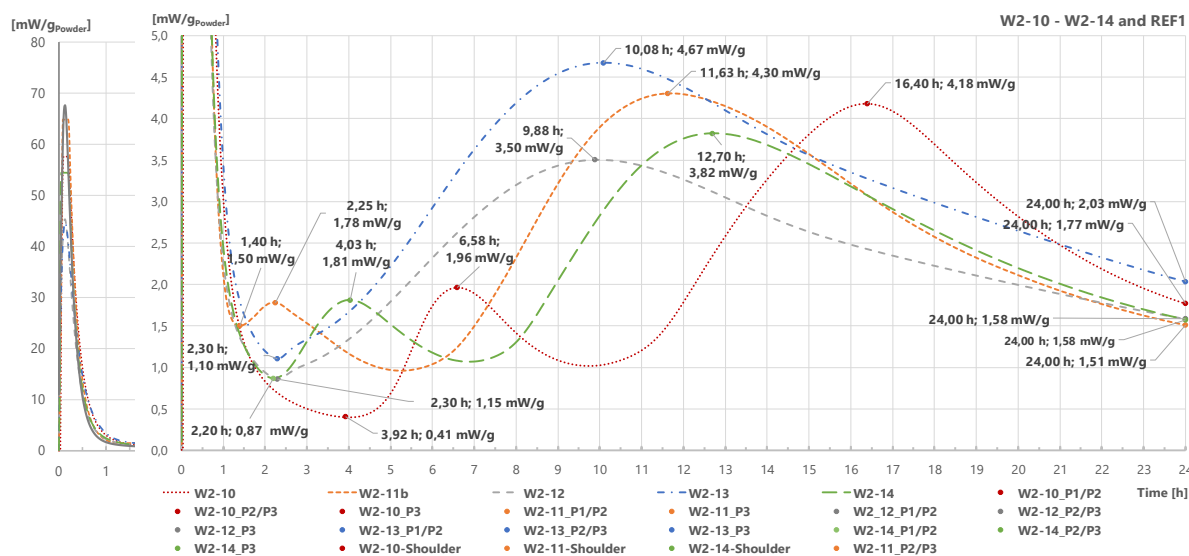


Figure 26: Heat of hydration of dry-mix shotcrete mortars with SPBM2 and other SCMs

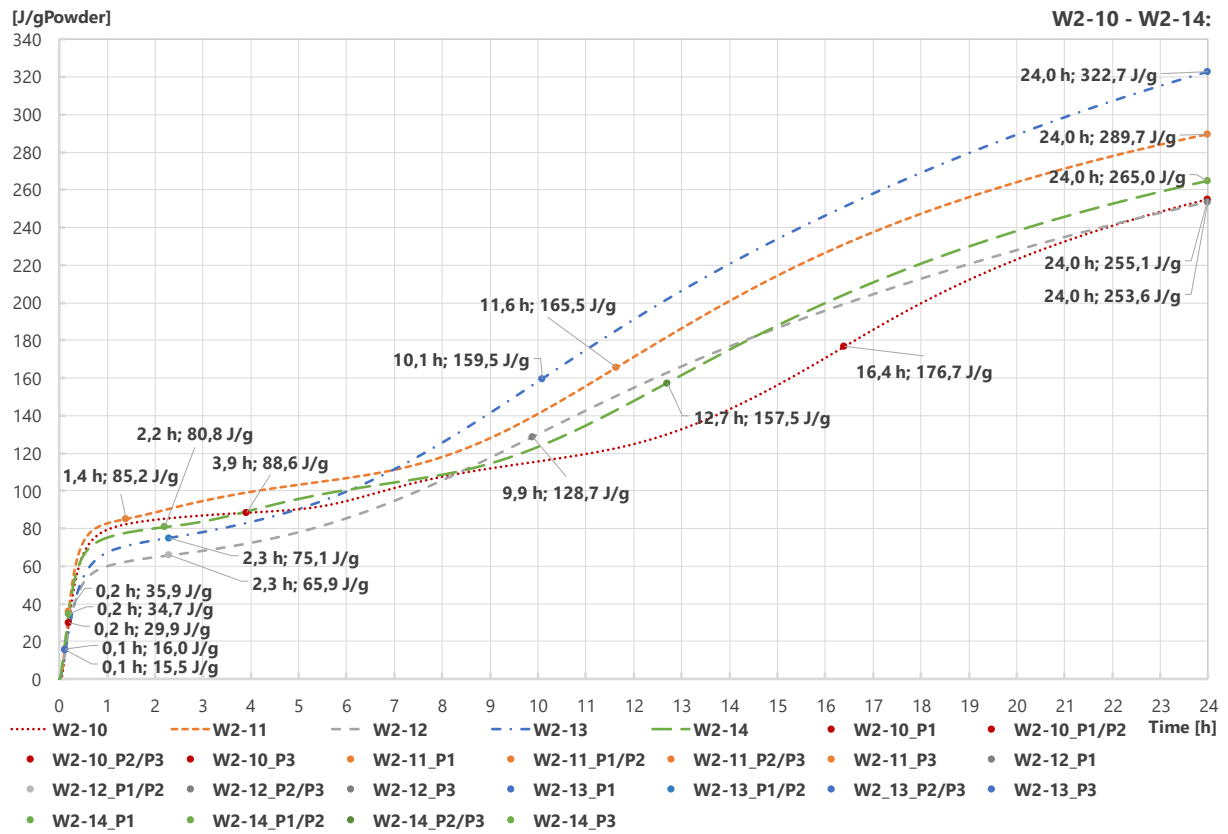


Figure 27: Cumulative heat of hydration of dry-mix shotcrete mortars containing SPBM2 and other SCMs

Periods:		W2-10	W2-11b	W2-12	W2-13	W2-14
Period I	Start [h]	0.00	0.00	0.00	0.00	0.00
	End [h]	0.20	0.20	0.13	0.13	0.20
	Δt [h]	0.20	0.20	0.13	0.13	0.20
	Power [mW/g] ^a	57.57	64.81	45.31	44.64	54.43
	Heat Release [J/g] ^a	29.90	35.93	16.01	15.45	34.71
Period II	Start [h]	0.20	0.20	0.13	0.13	0.20
	End [h]	3.92	1.40	2.30	2.30	2.20
	Δt [h]	3.72	1.20	2.17	2.17	2.00
	Power [mW/g] ^a	0.40	1.50	0.86	1.10	0.87
	Heat Release [J/g] ^a	88.60	85.16	65.86	75.08	80.85
Period III	Start [h]	3.92	1.40	2.30	2.30	2.20
	End [h]	16.40	11.63	9.88	10.08	12.70
	Δt [h]	12.48	10.23	7.58	7.78	10.50
	Power [mW/g] ^a	4.18	4.30	3.50	4.67	3.82
	Heat Release [J/g] ^a	176.72	165.49	128.75	159.46	157.46
Period IV	Start [h]	16.40	11.63	9.88	10.08	12.70
	End [h]	24.00	24.00	24.00	24.00	24.00
	Δt [h]	7.60	12.37	14.12	13.92	11.30
	Power [mW/g] ^a	1.77	1.51	1.58	2.03	1.58
	Heat Release [J/g] ^a	255.11	289.72	253.64	322.72	265.00

^a powder

Table 15: Summary of the hydration periods of dry-mix shotcrete mortar with SPBM2 and SCMs

Mixture REF-1 with SPBM2

Figure 28 shows the heat release of samples with 100% SPBM2 during a period of 24 hours. The progresses of all four samples shows distinct curve characteristics with their inflection points. This points identifies phase transitions between the stages of hydration. This can be seen for the cumulative heat progresses in Figure 29 too. The detailed results are shown in Table 16.

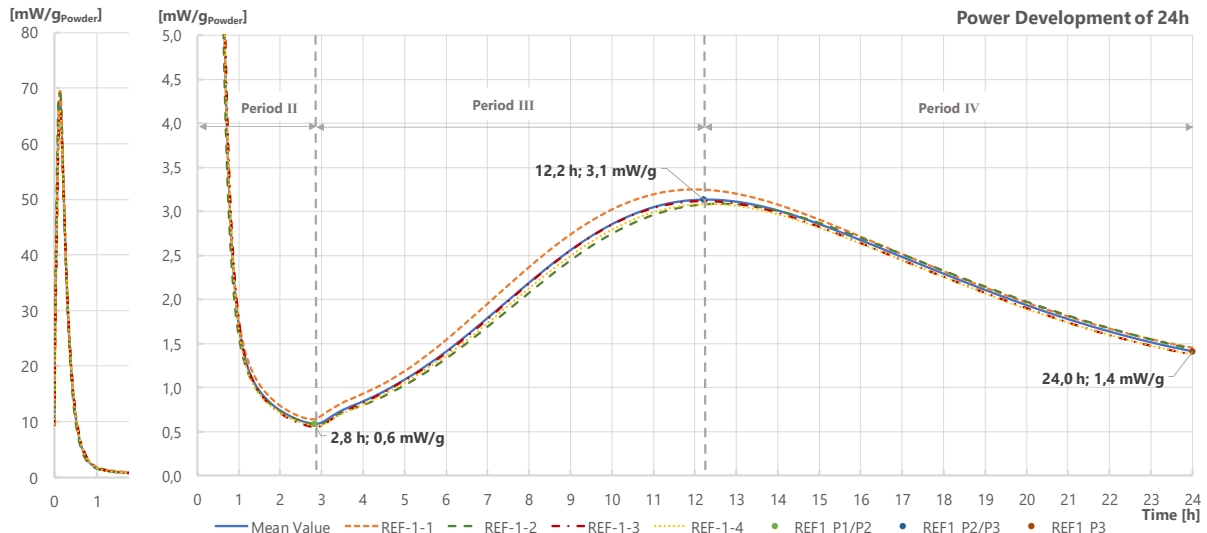


Figure 28: Heat of hydration of dry-mix shotcrete mortars with 100% SPBM2 and different sample sizes

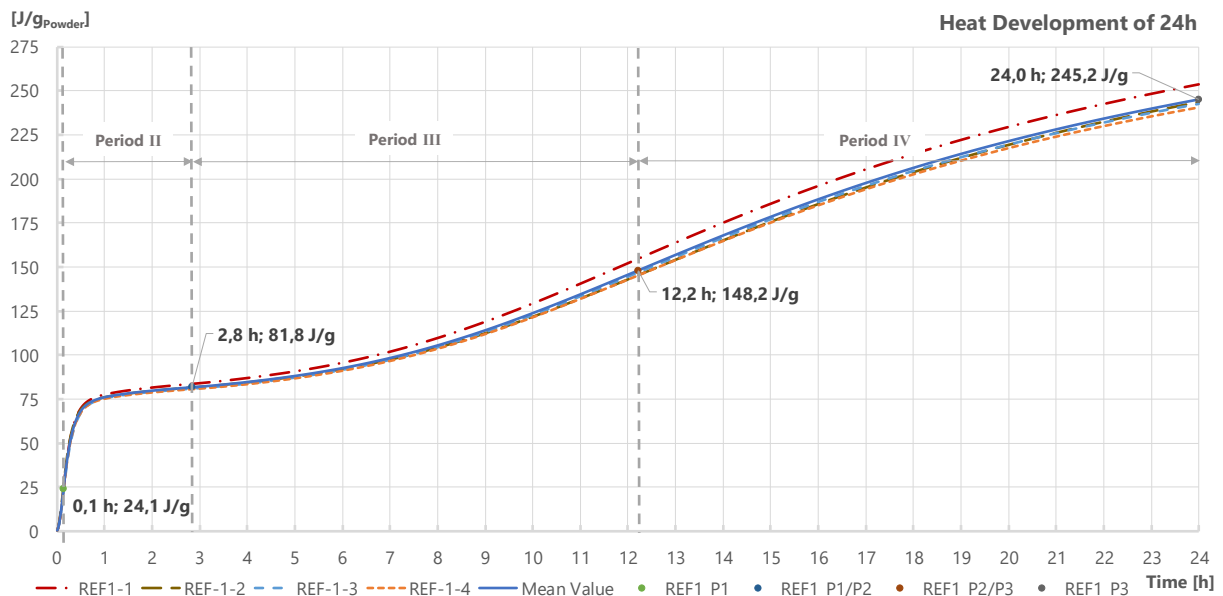


Figure 29: Cumulative heat of hydration of dry-mix shotcrete mortars containing 100% SPBM2 and different sample sizes

Periods:	REF 1	
Period I	Start [h]	0.00
	End [h]	0.13
	Δt [h]	0.13
	Power [mW/g]	67.60
	Heat Release [J/g]	24.09
Period II	Start [h]	0.13
	End [h]	2.83
	Δt [h]	2.70
	Power [mW/g]	0.58
	Heat Release [J/g]	81.80
Period III	Start [h]	2.83
	End [h]	12.22
	Δt [h]	9.38
	Power [mW/g]	3.13
	Heat Release [J/g]	148.16
Period IV	Start [h]	12.22
	End [h]	24.00
	Δt [h]	11.78
	Power [mW/g]	1.41
	Heat Release [J/g]	245.22

Table 16: Summary of the hydration periods of dry-mix shotcrete mortar with 100% SPBM2

Mixture REF-2 with CEM I SR0 and CAC

Figure 30 shows the complete heat release of samples with 90% CEM I 52,2N SR0 and 10% CAC SC1 during a period of 24 hours. The heat release progresses, equal to the results of REF-1, shows distinct curve characteristics with their deceive points. Even though the curves show an identical characteristic at period two to four, the initial peaks are different in height. The summarized results can be seen in Table 17.

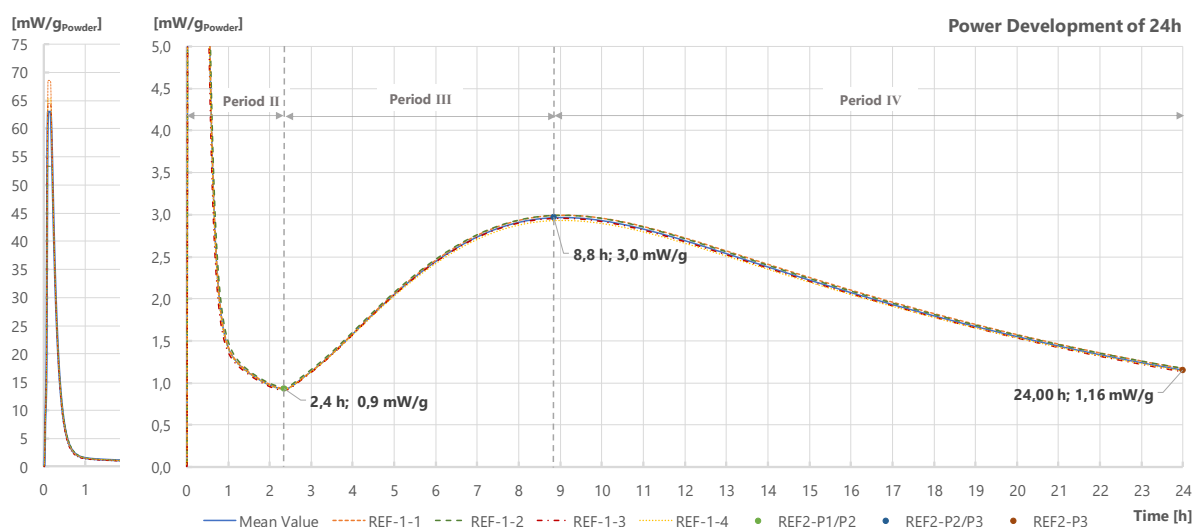


Figure 30: Heat of hydration of dry-mix shotcrete mortars with 90% CEM I 52.5N SRO with 10% CAC SC1 and different sample sizes

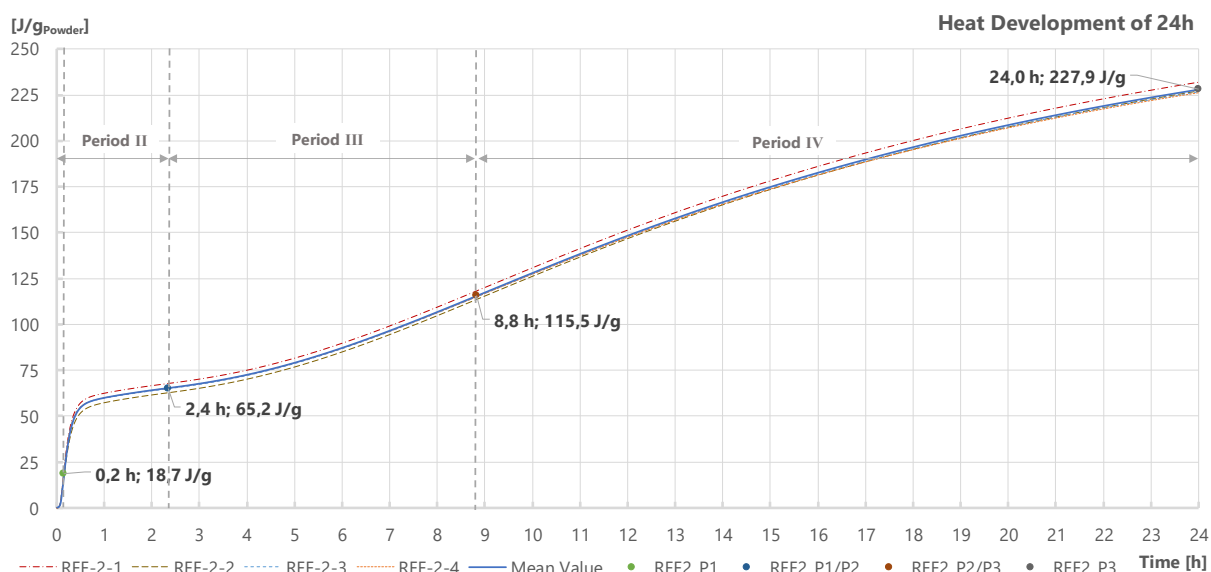


Figure 31: Cumulative heat of hydration of dry-mix shotcrete mortars containing 90% CEM 52.5N SRO with 10% CAC SC1 and different sample sizes

Periods:		REF 2
Period I	Start [h]	0.00
	End [h]	0.15
	Δt [h]	0.15
	Power [mW/g]	62.91
	Heat Release [J/g]	18.67
Period II	Start [h]	0.15
	End [h]	2.35
	Δt [h]	2.20
	Power [mW/g]	0.93
	Heat Release [J/g]	65.17
Period III	Start [h]	2.35
	End [h]	8.83
	Δt [h]	6.48
	Power [mW/g]	2.97
	Heat Release [J/g]	115.50
Period IV	Start [h]	8.83
	End [h]	24.00
	Δt [h]	15.17
	Power [mW/g]	1.16
	Heat Release [J/g]	227.94

Table 17: Summary of the hydration periods of dry- mix shotcrete mortar with 90% CEM I 52,5N SRO and 10% CAC-SC1

4.3 XRD

The hydration stages of REF1 and REF2 of in-situ XRD investigations are shown in 4.3.1 and 4.3.2. These moments are the changeovers, whereas water is added (0h), the initial peak occurs ($\approx 0.2h$), the transition from period I to period II, the transition from period II to period III and the last observation after about 24 hours (period III). In addition, the patterns are shown where CS-tests were made. This are at the first, the third and the sixed hour of hydration.

4.3.1 XRD-Investigations of REF1

The XRD pattern of REF1 is shown in the following Figure 32, Figure 33 Figure 34. Detailed information about the peak intensities can be seen in Table 18.

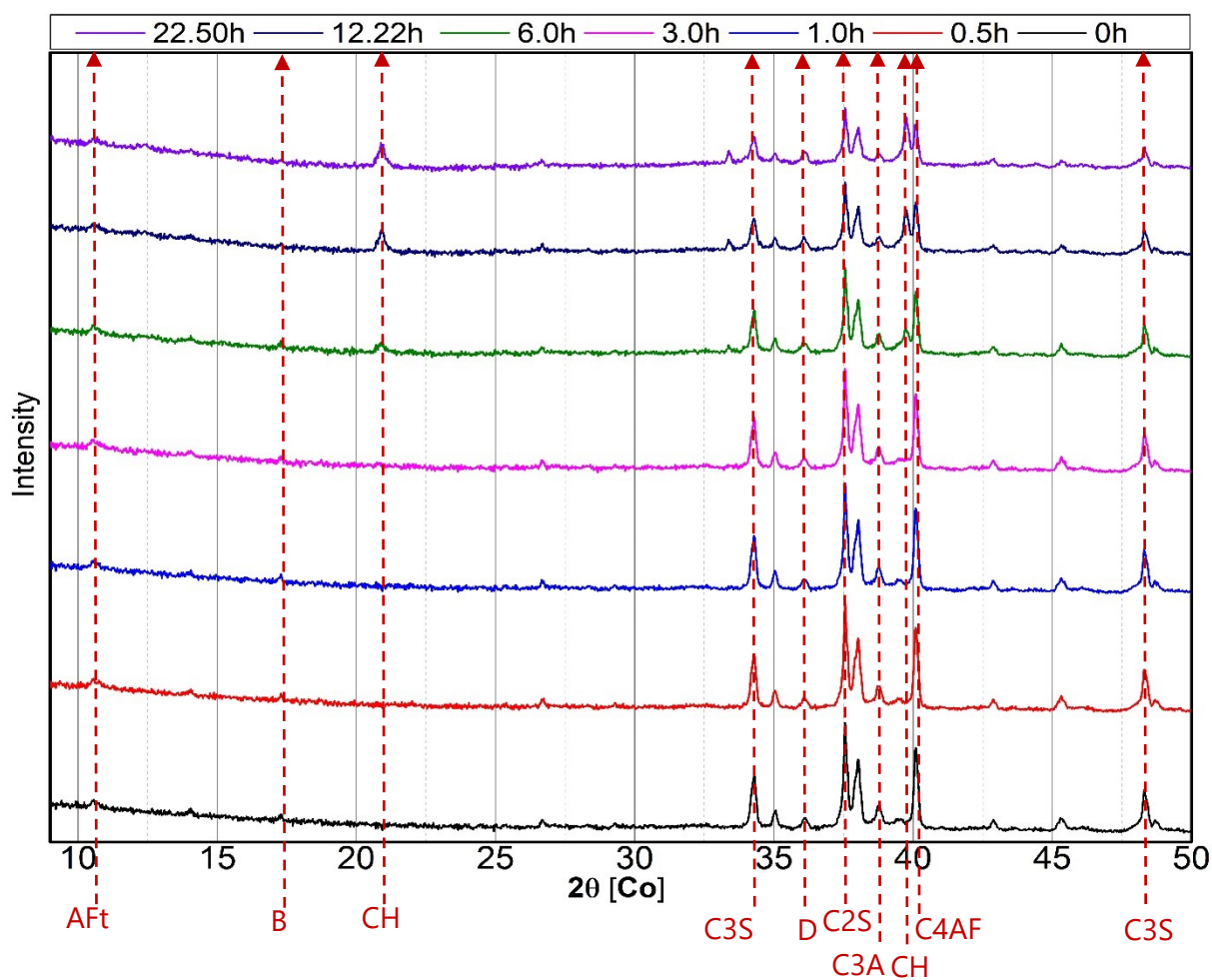


Figure 32: XRD-patterns of REF 1

No.:	Findings:	2θ (Co): ¹²
1	Ettringite (AFt)	10.54
2	Basanite (B)	17.13
3	Portlandite (CH)	21.03
4	Alite (C3S)	34.20
5	Ferrite (C4AF)	34.38
6	Dolomite (D)	36.17
7	Belite (C2S)	37.54
8	Aluminate (C3A)	38.77
9	Belite (C2S)	38.05
10	Portlandite (CH)	39.82
11	Ferrite (C4AF)	40.11
12	Alite (C3S)	48.40

Table 18: Findings of the in-situ XRD investigations of mixtures with 100% SPBM2

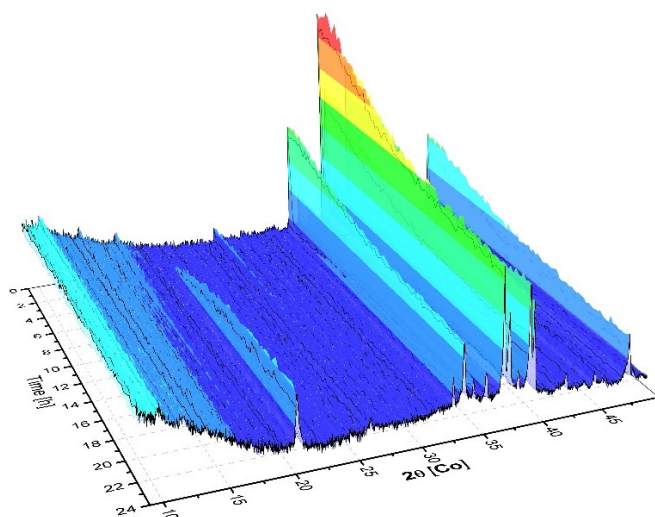


Figure 33: 24h in-situ XRD 3D-plot from 9-50 2θ° (Co) of mixture REF1

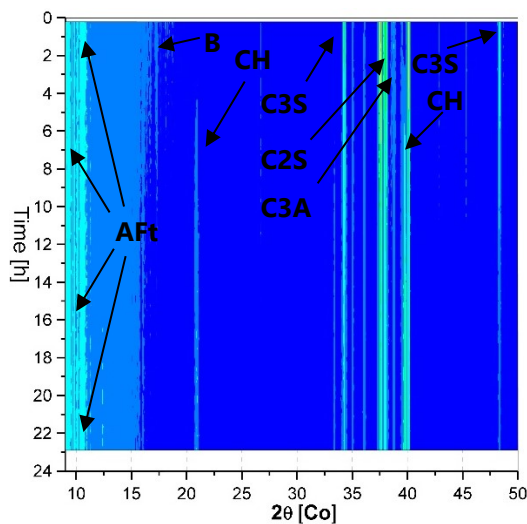


Figure 34: 24h in-situ XRD 2D-plot from 9-50° 2θ (Co) of mixture REF1

¹² AMCS D data base: <http://ruff.geo.arizona.edu/AMS/amcsd.php> [20.10.2018]

4.3.2 XRD-Investigations of REF2

The XRD pattern of REF1 is shown in the following Figure 35, Figure 36 and Figure 37. Table 19 displays detailed information about the peak intensities.

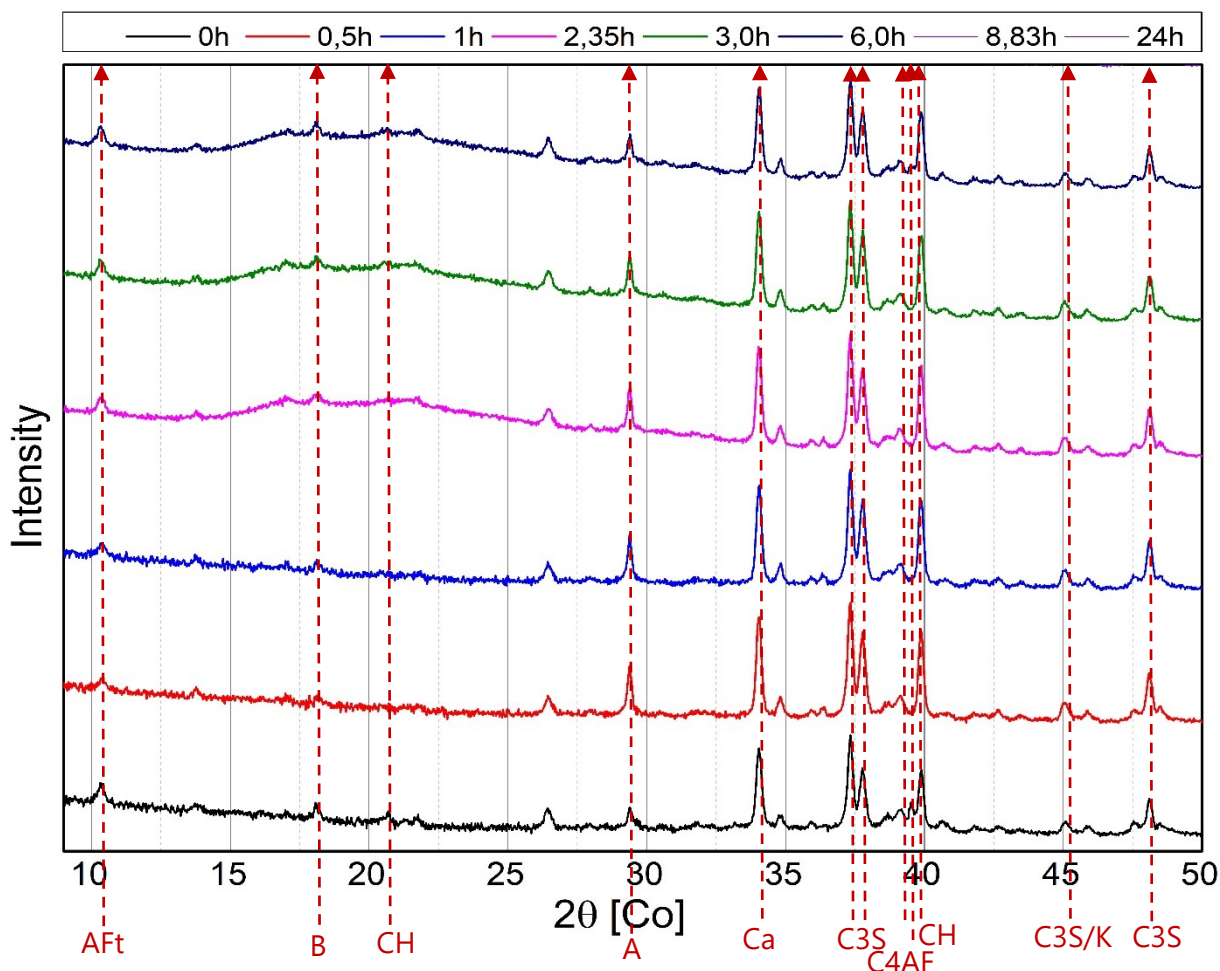


Figure 35: XRD-patterns of REF 2

No.:	Findings:	2θ (Co): ¹³
1	Ettringite (Aft)	10.54
2	Basanite (B)	17.13
3	Ettringite (Aft)	18.12
4	Portlandite (CH)	21.03
5	Anhydrate (A)	29.64
6	Calcite (Ca)	34.20
7	Alite (C3S)	37.54
8	Alite (C3S)	37.76
9	Ferrite (C4AF)	39.54
10	Portlandite (CH)	39.82

¹³ AMCS D data base: <http://rruff.geo.arizona.edu/AMS/amcsd.php> [20.10.2018]

No.:	Findings:	2θ (Co): ¹³
11	Alite (C3S)	39.86
12	Alite/Katoite (C3S/K)	45.88
13	Alite (C3S)	48.40

Table 19: Findings of the in-situ XRD investigations of mixtures with 90% CEM I SRO and 10% CAC SC1

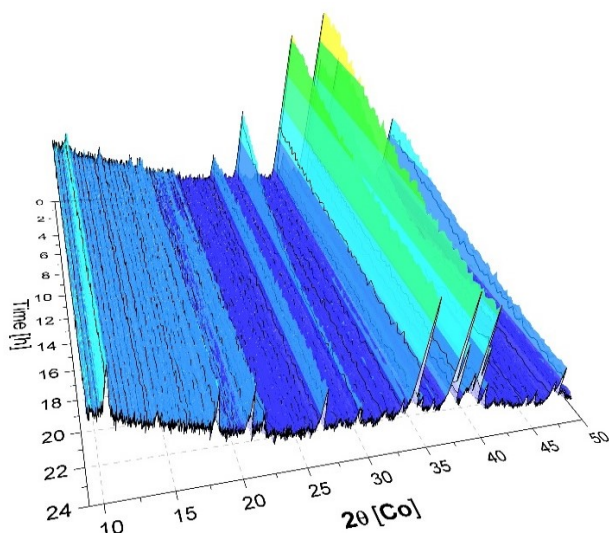


Figure 36: 24h in-situ XRD 3D-plot from 9-50° 2θ (Co) of mixture REF2

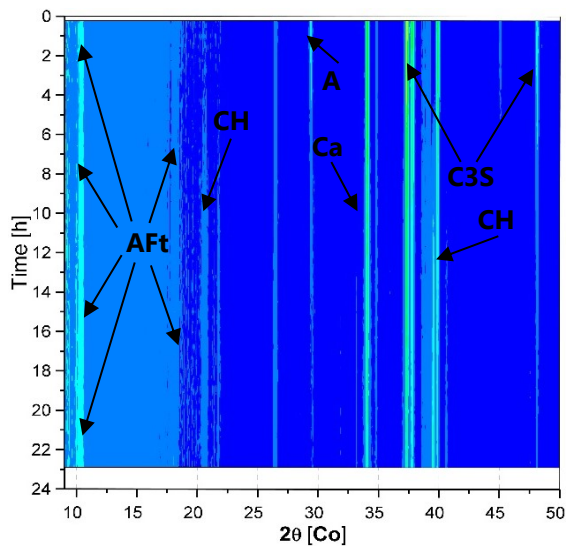


Figure 37: 24h in-situ XRD 2D-plot from 9-50° 2θ (Co) of mixture REF2

5 Analysis and Argumentation

Throughout the present work, dry-mix shotcrete mixtures were investigated in terms of CS, heat energy output and mineral growth in the early age of hydration. The following subchapters summarize and analyse the collected data. Therefore, all outcomes are ordered depending on their content of SRO or SPBM2.

5.1 Compressive Strength Development under Laboratory Conditions

The mixtures W2-03 and W2-04 were made with CEM I SRO cement containing both ten percent CAC SC1. Beyond that, mixture W2-04 contains 15 percent MEF HÜS 4500 and five percent MIF-CAL EGU. The result showed that the substitution of SRO-cement through MEF HÜS 4500 and MIF CAL EGU does not reduce the CS-results after six hours of hydration. On the contrary, mixture W2-04 shows slightly higher CS-values at the very early stage of hydration in comparison with W2-03. Presumptively, the slow latent-hydraulic reaction of MEF HÜS 4500 (contains C_2S) with CH can not be accountable for this early stage of hydration. In the opinion of the author, the very early increased CS-value is caused by the difference in grain size between all constituents especially of the micro filler MIF CAL EGU. It is assumed that, the inert filler effect, as described in (Matschei, Lothenbach, and Glasser 2007), lead to a denser packing and less space between the grains at this very early stage of hydration. The additional formation of AFt, caused by the additional CAL EGU could not be detected with the applied examination methods. The influence of CAC SC1 on the CS-development cannot be detected either, as both mixtures contain ten percent CAC SC1 each. The slightly higher CS-value after 28 days of W2-04 compared to W2-03 is in the deviation margin. Thus, an influence of one of the constituents on the later CS-behaviour cannot be seen. Noteworthy here is the degree of substitution of mixture W2-04.

The influence of additional constituents of mixtures W2-10 until W2-14 show a wider range. First, the influence of added CAC PP 222 to W2-10 cannot be seen at the very early stage of hydration. The CS-value is below that of REF1. Even the CS-value of the 24 hours test is much lower than the one of REF1. Only after 28 days, W2-10 reaches the CS-level of REF1.

In contrast to that, mixture W2-11b shows a significantly higher first CS-value in comparison with REF1. Though, W2-11b contains the same amount of SPBM2. The first distinction of W2-11b to W2-10 is the content of five percent of CAC-SC1 and five percent CACPP 222 instead of ten percent of CAC-PP-222. The second main distinction is the effect of five percent of a micro filler MIF MET SF with its much lower grain diameter. After 24 hours of hydration, the mixture W2-11b shows a lower CS-value in comparison to the reference REF1. Only then, after 28 days, the CS is obviously higher again compared to the reference. This might be caused by the additional C_2S from the GGBFS, which has a slower reaction rate. However, the later CS-values are low in comparison to the other mixtures. The relative high early CS and the lower increase at later stages complies with (Scrivener 2003, 2/26).

The mixture W2-12, which consists of 75 percent SPBM2 shows a lower first CS-value compared to the reference REF1 and W2-11b. The slightly higher amount of SPBM2, in comparison to the other mixtures, does not lead to a higher CS-value. Furthermore, the additional admixtures CAL EGU and MIF MET SF shows obviously no effect during the first 24 hours of hydration. The CS-value increases significantly eventually after 28 days of hydration and exceeds REF1 and even W2-11b. According to (Le Puerta-Falla 2015), this is probably caused by the additional CAL-EGU in combination with MIF-MET. On one side, because of the pozzolanic character of metakaolin and on the other side because of the activation of the CAL-EGU through the aluminium content of metakaolin.

The next mixture W2-13 was not workable at a W/B-value of 0.50. The specific feature of this mixture was the added plasticiser. It increases the flowability during the production process greatly and it was necessary to reduce the W/B-value up to 0.38. This reduction made it complicated to compare the results from this mixture with all the other investigated mixtures in the first glance. The lower W/B-ratio affects

the CS-development, in terms of dry-mix shotcrete, at later stages of hydration (24 hours till 28 days). Both, the CS-value after 24 hours and 28 days were the highest measured values in the whole study. This shows the high influence of the W/B-value on the CS-development. Findings in (Bentz, Peltz, and Winpiger 2009) confirms this influential factor at later stages of hydration. However, the earliest CS-result (at six hours) did not show the highest CS-result of all investigated mixtures at this time. This may indicate a higher influence of SCMs, than a reduced W/B-value during the first hours of hydration. In the opinion of the author, further investigations should be performed, whereas a reduced W/B-value in combination with a plasticiser is added to the other mixtures to analyse the CS-development.

The blend W2-14 is a composition of 50 percent SPBM2, three percent CAC SC1, 30 percent MEF HÜS, five percent CAL EGU, seven percent CAC PP 222, five percent MIF MET SF and 0.8 percent of a plasticiser. This mixture has the lowest early age CS-value of all investigated blends, although it contains CAC. However, the amount of SPBM2 is low and within the contained calcium sulphate, which is necessary for the reaction of CAC. Thus, advantages of the added CAC cannot be utilised. Otherwise, the mix made up leeway after 28 days of hydration. The CS-value strongly increases, surpasses REF1 and achieves almost the level of W2-12. The reason for this rise might be caused by the relatively high amount of MEF HÜS 4500 (30 percent) and within a high amount of C_2S .

Further detailed analysis of REF1 and REF2 showed that the CS-development in the period between one and three hours of hydration decelerates. The first main CS-development happens in the first hour of hydration. The next nameable CS-growth could be detected during the sixed and 24th hour. The observation shows a dormant period during the hydration. This phenomenon could be detected at both mixtures independent if SPBM2 or CEM I SRO with CAC was investigated.

5.1.1 Laboratory - versus Full-Scale Test

The data in Table 20 compares the results from the laboratory with those from the full-scale test. The results have one thing in common. All mixtures, which were made in the lab except for W2-11b, have significantly lower CS-values compared with the ones from the full-scale test after six hours. Even the results after 24 hours and 28 days show this tendency, even though the differences get lower. In contrast to that, mixture W2-11b shows a much better performance compared with W2-11 from the full-scale test. This must be caused through the added five percent of CAC-SC1 instead of five percent CAL-EGU. The samples W2-13 and W2-13 from the full-scale test showed equal CS-developments. This draws the conclusion that there may be some other influencing factors that exist, which lead to lower CS-values in the laboratory. The compacting energy is a noticeable parameter. The generated dynamic energy during the spraying was much higher than the compacting energy, which was generated through the external vibrator in the laboratory. The different amounts of compacting energies can be seen in Figure 38 and Figure 39. The sample on the left shows obviously more air voids than the sample on the right from the full-scale test. This observation agrees with findings in (Salvador et al. 2016), where researches were done with sprayed accelerated cement pastes.

In addition to that, the W/B-ratios, which can be seen for the full-scale test at 3.2.2, were slightly lower than those from the test in the laboratory. Another important driver were the different types of aggregate and their different grain-size distributions, which are shown in 3.2.1 and 3.3.2. A better correspondence with the idealistic maximum density curve can be seen for the aggregate from the full-scale test. Disregarding these conditions, examinations in (Shuang Zhang, Yong Ma, and Teng Han 2010) indicate, that the storage period influences the dry-mix material. Their investigation showed a declined reactivity and within lower CS-values over time. This can be a further reason for lower CS-values at the laboratory. The time lab of approximately three to six months during this current investigation can be a relevant factor for objective results. In the opinion of the author, all these factors affected the pore structure and led to higher CS-values at the full-scale test.

No.:	Shortcut:	Full-Scale-Test:			Laboratory Test:		
		6h [N/mm ²]	24h [N/mm ²]	28d [N/mm ²]	6h [N/mm ²]	24h [N/mm ²]	28d [N/mm ²]
W2-03	90%SRO 10%CAC-SC1	4.50	18.07	66.30	2.51	17.84	47.94
W2-04	70%SRO 10%CAC-SC1 15%HÜS 5%CAL	8.00	20.64	78.20	3.27	17.08	50.81
W2-10	70%SPBM-2 20%HÜS 10%CAC-PP	8.80	22.46	60.30	1.65	12.53	35.39
W2-11	70%SPBM-2 5%CAC-SC1 15%HÜS 5%CAL EGU 5%MET	2.50	8.85	57.50	--	--	--
W2-11b	70%SPBM-2 5%CAC-SC1 15%HÜS 5%CAC-PP 5%MET	--	--	--	3.35	16.56	40.25
W2-12	75%SPBM-2 15%HÜS 5% CAL EGU 5%MET	3.00	19.53	69.80	1.28	15.53	45.60
W2-13	70%SPBM-2 20%HÜS 10%CAL	5.10	20.27	74.80	2.50	26.65	58.58
W2-14	50%SPBM-2 3%CAC-SC1 30%HÜS 5%CAL 7%CAC-PP	4.50	17.74	63.20	1.02	9.32	46.18
REF-1	100%SPBM-2	--	--	--	2.15	19.32	36.95
REF-2	90%SRO 10%CAC-SC1	--	--	--	2.57	19.19	51.09

Table 20: Comparison of full-scale-test-results with results from the laboratory tests



Figure 38: Samples which was made in the laboratory

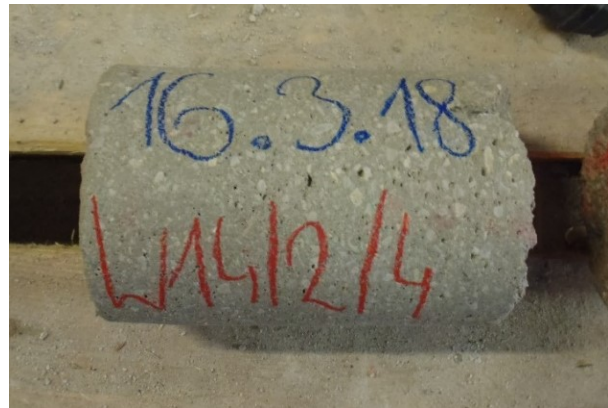


Figure 39: Cylindrical sample cut out from a sample produced at the full-scale test

5.2 Calorimetry

The heat release during hydration, as described in 2.1.3 and 2.3.1, occur because of an exothermic reaction. The kinematics of hydration depends on the properties (for example grain-size distribution or w/c-ratio) and respectively on the components of a mixture.

The heat flow-progress ($\text{mW/g}_{\text{powder}}$) showed equal periods of hydration, as it was detected by (Jiong Hu, Zhi Ge, and Kejin Wang) in there research. In particular, only mixtures containing CAC PP222 showed an additional but smaller peak during the acceleratory period. On the other hand, mixtures, which contained CAC SC 1, did not show this development. Furthermore, the substitution influences the height of peaks and shifts time spans of the hydration periods.

As shown in Figure 40 and Figure 41, it stands out, that mixtures W2-04, REF2 and W2-10 have a very early and short endotherm phase. This might be similar to findings in (Hewlett and Lea 2001, 269–70) for OPC, whereas small amounts of K^+ lead to a tiny initial endothermic peak right after the mixing process. On the other hand, these are fitted curves and data are very poorly available for this stage of hydration. Therefore, this should not be taken for granted.

Another feature can be seen at mixtures which containing CAC, independently of CAC SC1 or CAC PP. At the end of phase I, the graphs show plateaus. This aspect is due to a limitation of the calorimeter with its measurable maximum of 1.1 watts. The previous named blends developed a very strong heat liberation and exceeded the maximum measurable maximum of the calorimeter. This measuring inaccuracy was neglected in further calculations.

Table 21 shows the heat release by phase and time. The highest heat release rates per time occurs during phase one and phase two. The development decreases afterwards. The amount of heat liberation during the acceleration period (phase III) is equally high as during the initial and dormant stage (phase I and II), which continues just five to 15 minutes. The heat release per time increases slightly afterwards in phase IV again. It can be said, that about 30 percent of the total amount of released heat, which occurs within the first 24 hours, is released during the first 15 minutes (phase I and II). About 26 percent occur in phase III and circa 44 percent are generated in phase IV.

Further on, the comparison among all SCMs in Table 22 show a general tendency, that CACs, regardless from the specific product (CAC-SC1 or CAC-PP-222), liberates the most heat at six and 24 hours. On the contrary, mixtures which containing CAL-EGU in combination with MIF-MET-SF, liberated the lowest amount of heat after six hours. The raised heat liberation at the end of the observation period may indicates the activation of the reactivity of CAL-EGU in combination with MIF-MET-SF as its aluminous source. This investigation agrees with findings of (Antoni et al. 2012), where mixtures of OPC, partly substituted with limestone and metakaolin, showed a later CS-development.

Ser. No.:	Phase I & Phase II		Phase III		Phase IV	
	Heat Release / Phase	Heat Release / Time	Heat Release / Phase	Heat Release / Time	Heat Release / Phase	Heat Release / Time
	[J/g]	[J/gh]	[J/g]	[J/gh]	[J/g]	[J/gh]
W2-03-1	71.56	33.03	55.10	8.54	121.01	7.97
W2-04-1	81.18	27.06	38.03	7.00	103.57	6.73
W2-10-1	88.60	22.62	88.13	7.06	78.38	7.60
W2-11b-1	85.16	60.83	80.33	7.85	124.23	10.05
W2-12-1	65.86	28.64	62.88	7.58	124.89	8.85
W2-13-1	75.08	32.65	84.38	10.84	163.26	11.73
W2-14-1	80.85	36.75	76.61	7.30	107.54	9.52
REF-1	81.80	28.87	66.36	7.07	97.06	8.24
REF-2	65.17	27.73	50.33	7.76	112.44	7.41

Table 21: Heat release by phase and heat release by time for each phase of hydration

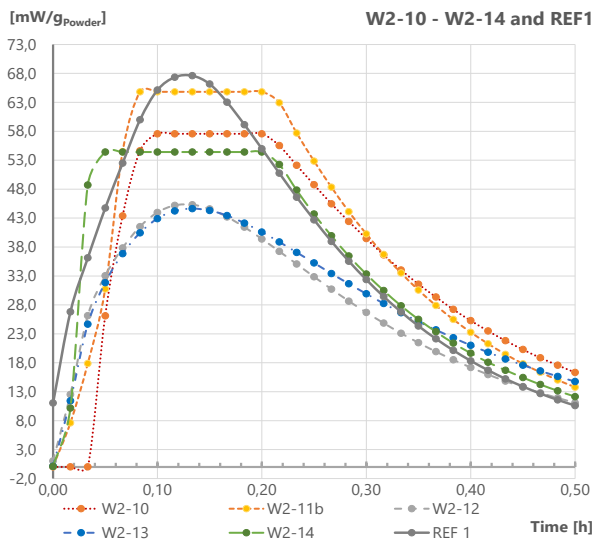


Figure 40: Initial peaks of mixtures with SPBM2

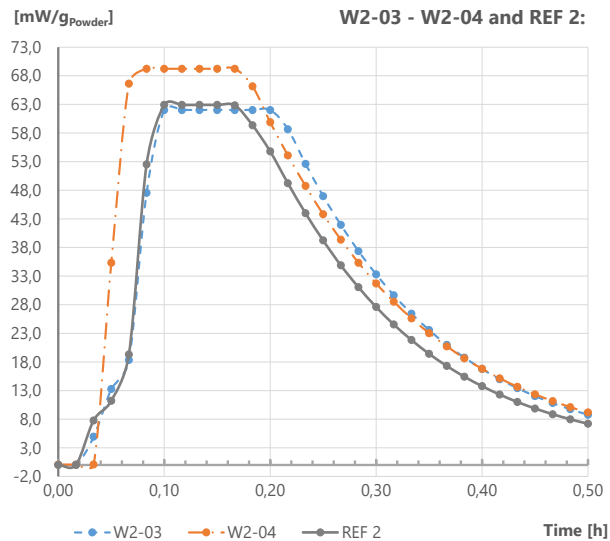


Figure 41: Initial peaks of mixtures with CEM I SRO

Ser. No.:	Cumulative heat per mass powder	
	6h [J/g]	24h [J/g]
W2-04-1	95,69	222,78
W2-10-1	94,82	255,11
W2-11b-1	106,86	289,72
W2-12-1	85,53	253,64

Table 22: Comparison of cumulative heat progresses

5.2.1 Correlation: Heat Release – Compressive Strength

As shown above, the combinations of a dry-mix powder and water lead to exothermic chemical reactions. The collected data from the calorimeter and from the CS-tests are compared with each other in Figure 42. This correlation shows a correlation coefficient of about 0.88. This correlation coefficient demonstrates a general linear tendency that a rise of CS is associated with an increase of released heat, which is associated with degree of hydration, equal to the results from (Schutter and Taerwe L. de 1996). Moreover, the findings are in accordance with (Bentz et al. 2012) conjecture of a linear relationship between CS and heat release.

Nevertheless, it should be underlined that the W/B-value of mixtures W2-13 is reduced and was made at a value of 0.38. Regardless of that, the mixtures W2-14 have a very low content of SPBM2. On the one hand, this may lead to a higher liberation of heat. On the other hand, the low CS-values at this time may come from the small amount of available clinker minerals, a higher content of admixtures and in general because of finer particles. This is equal to findings in (Jiong Hu, Zhi Ge, and Kejin Wang) and especially in (El-Hadj Kadria et al. 2011) where heat of hydration is mainly influenced by the finesse of the particles. The fitted line from all data has a slope of about $10.09 \text{ Jmm}^2/\text{Ng}$ and intersects the ordinate at 75.86 J/g . This implies that the first CS-development starts at approximately 0.2 hours of hydration. This was generally the time when the initial peak was exceeded.

However, Figure 43 shows a more precise correlation of mortars which consisting of 100 percent SPBM2. The fitted line from all data has a slope of about $9.11 \text{ Jmm}^2/\text{Ng}$ and intersects the ordinate at 69.4 J/g . The correlation coefficient shows a very strong linear relationship between heat release and CS-development at a first glance, but a more accurate statement needs more date during the time from the sixed and twelfth hour of hydration. However, the following linear equation (21) can be used for a first and fast estimated CS-value through the data from a calorimeter investigation.

The next Figure 44 shows a precise correlation of mortars which consisting of 90% CEM I SR0 and 10% CAC SC1. It can be seen that, the fitted line from of the collected data has a slope of about $8.92 \text{ Jmm}^2/\text{Ng}$. The line intersects the ordinate at about 57.41 J/g . The correlation coefficient, as found in the previous mixtures, shows a very strong linear relationship between heat release and CS-development. Even though, a more accurate statement needs more data during the time from the third and ninth hour of hydration. Nevertheless, the following linear equation (22) can be used for a first and fast estimated CS-value through the data from a calorimeter investigation.

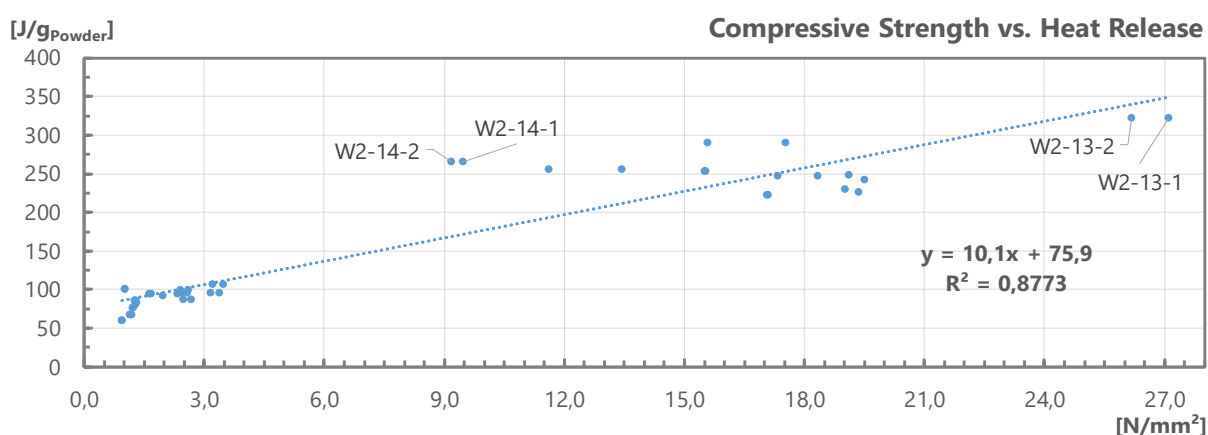


Figure 42: Heat Release vs. Compressive Strength of all tested samples

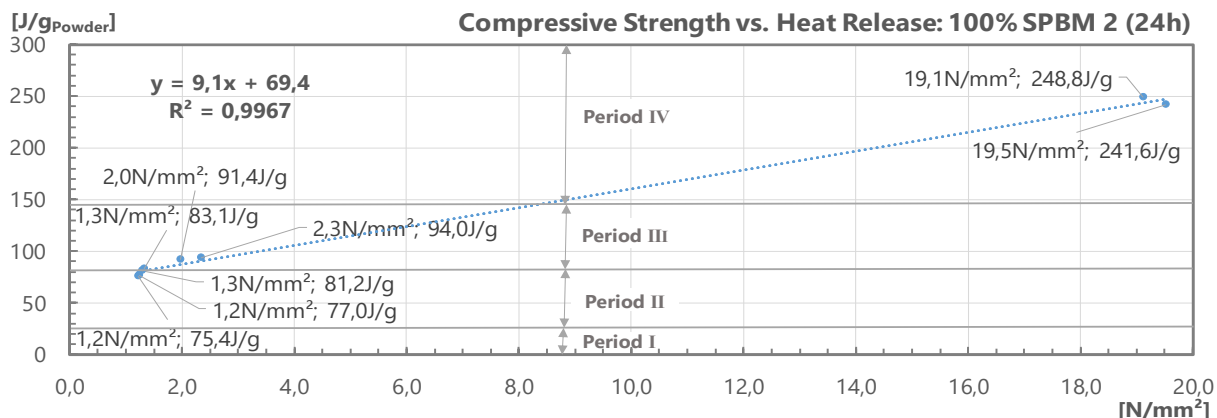


Figure 43: Heat Release vs. Compressive Strength of tested mortars consists of 100% SPBM2

$$\frac{y - 69.4}{9.1} = x \quad \left[\frac{N}{mm^2} \right] \quad (21)$$

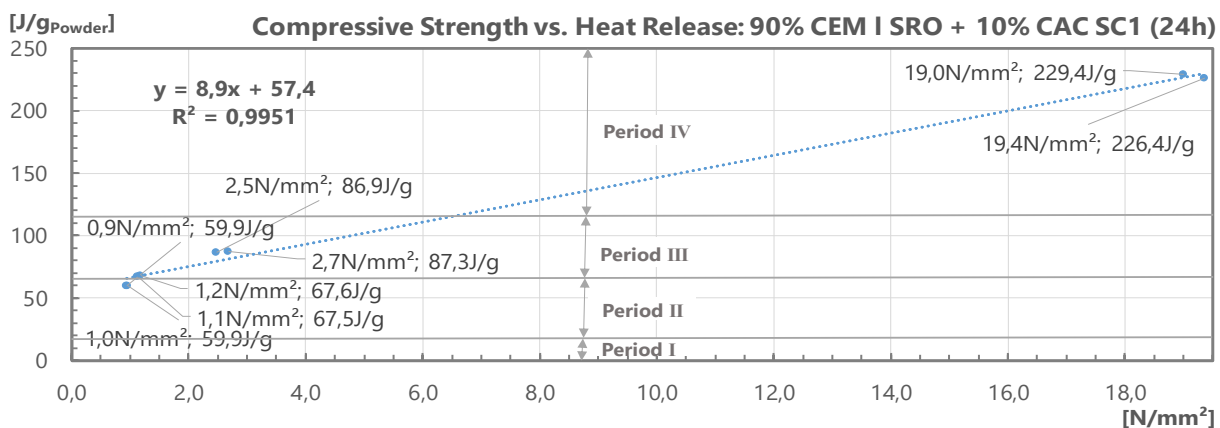


Figure 44: Heat Release vs. Compressive Strength of tested mortars consists of 90% CEM I SRO and 10% CAC SC1

$$\frac{y - 57.412}{8.9154} = x \quad \left[\frac{N}{mm^2} \right] \quad (22)$$

5.3 XRD

REF 1:

The illustration Figure 45 displays the observed intensity development of preselected crystalline structures over about 24 hours of hydration of REF1. A general decrease of initial crystalline phases can be observed over time. In general, it is understood, in consonant with (Choudhary et al. 2015), that this decrease comes along with an increase of amorphous CSH-phases. In more detail, a small amount of ettringite is seen from the first minutes on. This indicates a swift reaction of C_3A with calcium sulphate in the form of basanite (SO_3 ; 1.2%), which is part of SPBM2. The results show a decreasing and then a stagnating intensity of basanite, during period III. In order to the stagnating formation of new ettringite, it can be assumed with reasonable certainty that mostly everything of the basanite in the mixture is consumed. This is the period where the acceleration period ends, cf. 0. According to the postulated CSH_2/C_3A -ratio from (Stark and Wicht 2000, 191–93) there must be a further reaction of C_3A to mono-sulphate and perhaps CAH, cf. 2.1.1. This monosulphate could not be detected during the observation period of about 24 hours.

Moreover, similar to findings of (Choudhary et al. 2015), alite and belite start decreasing very rapidly at approximately during 1.5 and 2.3 hours of hydration. Both constituents follow this tendency continuously at least until the end of the observation period. The first detected portlandite in REF1 could be detected between 2.0 and 2.8 hours of hydration. This coincides with the end of the dormant- and the beginning of the acceleration period, which occurs at that time. The formation of portlandite is associated with the formation of amorphous CSH, cf. 2.1.1. Therefore, this must be nearly the starting point at which CSH-phases occur. The formation of portlandite and the decrease of alite and belite attenuates in the post-acceleration period again.

REF 2:

The Figure 46 shows the observed hydration process over the first 24 hours of REF 2, which contains 90 percent CEM I SR0 and ten percent CAC SC1. The aluminat reaction of C_3A led to a rapid formation of ettringite. The AFt was found from the first minute on, even though the intensity of this formation almost stagnates and holds its level during the first 24 hours. At the same time, the amount of calcium sulphate decreases. In more detail, it can be seen in Figure 46, that the amount of anhydrate decreases. Despite of that, the content of Basanite stagnates and holds its level. The examination of (Nehringa et al. 2018) studied, among other mixtures, a comparable mixture which contained 85 percent OPC and 15 percent CAC. Nehringer et al. even found ettringite first during the initial period. They associated the formation of ettringite with the decrease of C_3A , CAC and anhydrite.

The amount of alite decrease over time and instead of that, portlandite starts to occur approximately during 2.0 and 2.5 hours of hydration. This is the transition point where the dormant period ends and the acceleration period begins. This trend last until the end of the observation period. It is assumed that the occurrence of portlandite is in accordance with the formation of CSH-phases. These findings are in inconsistency with observation of (Nehringa et al. 2018). Nehringa et al. detected a low alite dissolution during the first 30 hours, though no associated precipitation of CSH and portlandite. Further, they detected portlandite first after 46 hours of hydration.

Independently from that, calcite was detected, which is part of the CEM I SR0. It was depleted quite constantly over the first 24 hours. In opinion of the author, this depletion is caused by the additional amount of aluminium from the CAC. The reactive capacity of the calcite was activated and a pozzolanic reaction took place and the ions from the calcite react with the CAC. This assumption is in accordance with findings of (Bizzozero and Scrivener 2015).

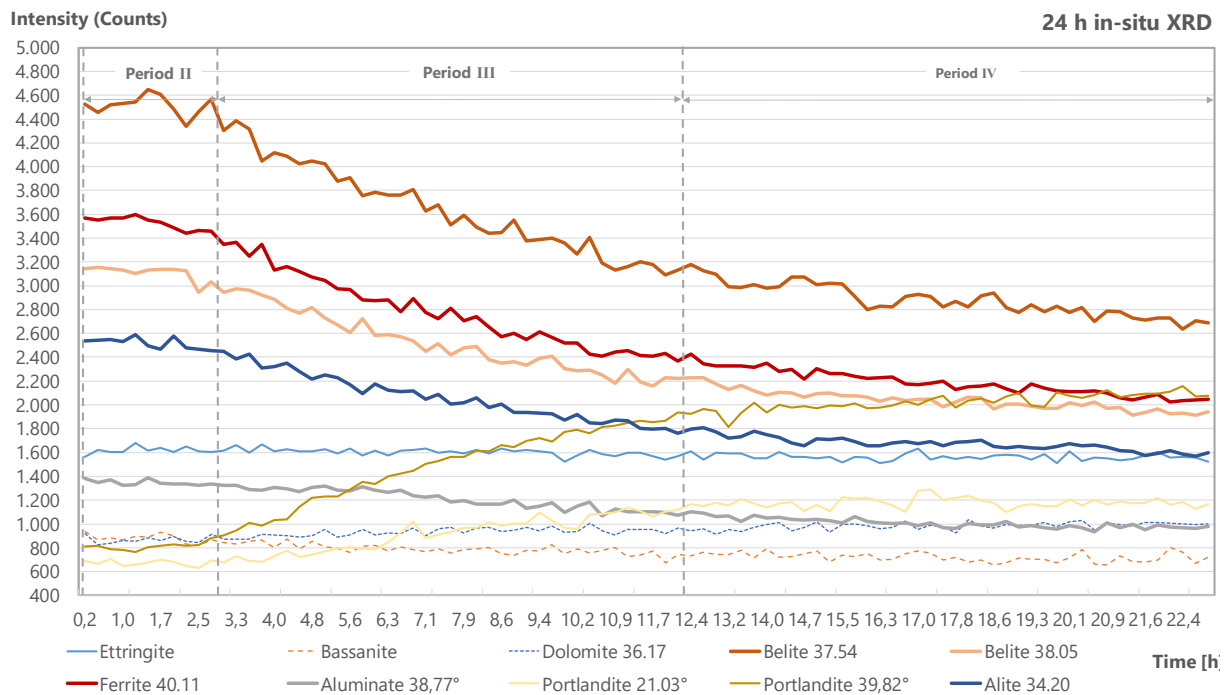


Figure 45: Intensity trends during the ongoing hydration of REF1

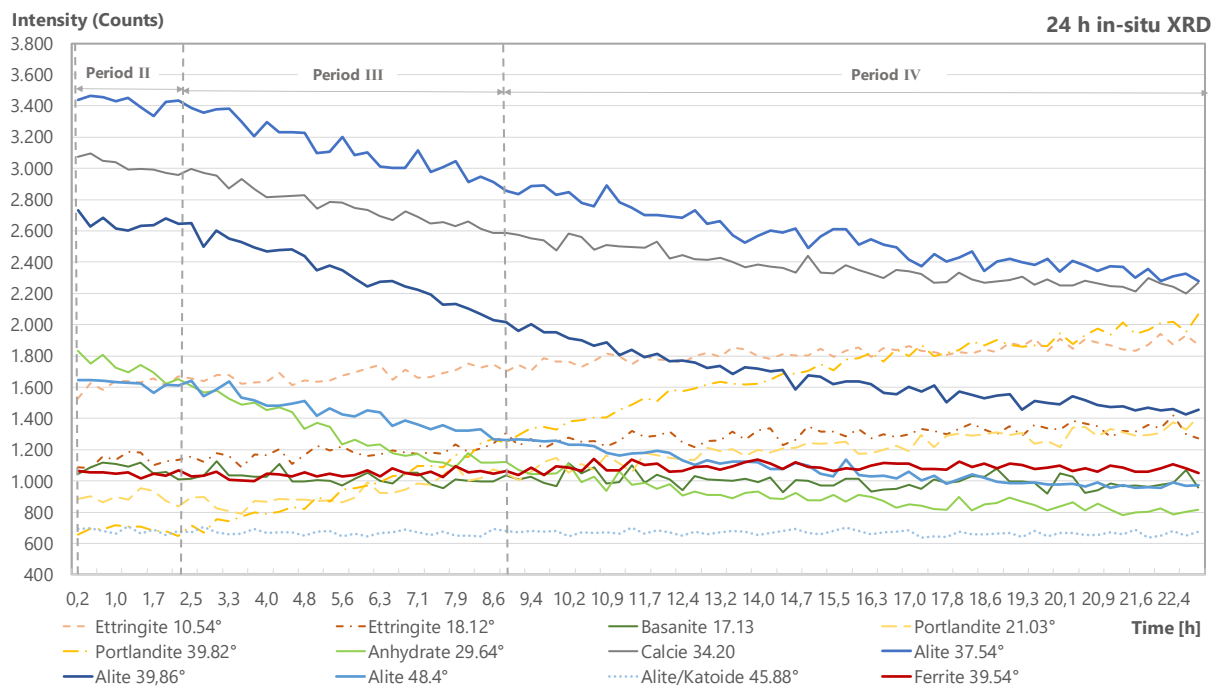


Figure 46: Intensity trends during the ongoing hydration of REF2

6 Conclusion

The primary aim of this master thesis was to investigate the early-age compressive strength development of dry-mix shotcrete according to different SCMs and admixtures. The results have indicated that a substitution of CEM I SRO or SPBM2 with about 30 percent of SCMs or admixtures lead to comparable CS-results, if about five to ten percent of CAC SC1 is present. The positive effects of CAL EGU on the very early-age compressive strength, which was determined in (Briendl et al. 2018) for wet-mix shotcrete could not be detected for dry-mix shotcrete. Even though, a filler effect cannot be excluded. Identically to that, the effect of metakaolin on the very early-age compressive strength could not be seen whether there maybe is a filler effect. However, mixtures with additional CAL EGU and metakoline lead to increased CS-values at later stages (28 days). This is perhaps caused through a pozzolanic reaction of metakaolin itself and the activation of CAL EGU through the additional metakaolin as its aluminous source. Nonetheless, the positive effect on the very early-age compressive strength development of CAC could be confirmed. Although, there is a remarkable difference between CAC SC1 and CAC PP222. The results show that mixtures containing CAC SC1 reach the highest compressive strength rates at the very beginning. On the other side, mixtures with CAC PP222 did not show such well behaviour. Only the combination with CAC SC1 led to compressive strength rises. The contrasting juxtaposition of result from the laboratory with those from the full-scale test showed a general tendency. The CS-results, measured in the laboratory, are always, with except of one, outrun by the results of the full-scale test. In opinion of the author, this is mainly caused by a higher compacting energy, which occurs during the spraying process. Further, the longer storage period of the SCMs as described in (Shuang Zhang, Yong Ma, and Teng Han 2010) cannot be excluded as an influencing factor. Another parameter is the W/B-value. The mixtures from the full-scale test exhibited approximately a six percent lower W/B-value. Those facts led, in combination with a different grain-size distribution, to higher compressive strength results at the full-scale test. However, as already mentioned, the only exception was mixture W2-11b. The only distinction of this mixture, in comparison with the one from the full-scale test, was the content of five percent of CAC SC1 instead of five percent of MIF CAL EGU. This distinction led to an increased very early CS-value. The result from the laboratory reached a 34 percent higher CS-value in comparison with the value from the full-scale test, independent from the compacting energy and the age of the base material.

Another target of this work was the investigation of thermodynamic reactions during the hydration process. The observations of dry-mix shotcrete displayed hydration periods, as it can be seen during the hydration of OPC. Besides of that, each mixture shows its own characteristics. The shape of the heat release curves, the peak heights, the duration of each period and even the number of all peaks was affected by the content of SCMs. In addition to that, only mixtures, which contained CAC PP222, showed an additional peak during the acceleration period. The reason for this phenomenon could not be clarified yet, and should be part of further research. The correlation of the date from the isothermal calorimeter and the result from the compressive strength test showed a positive tendency of CS and heat release. A more detailed contemplation of REF 1 and REF 2 showed a strong coherence of released heat energy and the compressive strength development. Based on this relation, further investigations on compressive strength of dry-mix shotcrete can be made more expeditiously. The linear function, which was found, during this investigations, conforms findings of (Bentz et al. 2012) and (Schutter and Taerwe L. de 1996). The findings can be used for dry-mix shotcrete mortar made in the laboratory. However, the approach, which was examined in the laboratory, can be adapted to the professional practise.

The last aim was to analyse the transformation of two dry-mix shotcrete samples REF 1 and REF 2 during the hydration process. Therefore, in-situ XRD observations were made over the first 24 hours of hydration. Mixture REF 1 was characterized first by the aluminat reaction. A small amount of basanite in the base material led to the formation of ettringite. A further formation of monosulphate or CAH. was not found during the first 24 hours of hydration. The following main reaction was the silicate reaction. Alite and belite decreases and portlandite was found at the end of the dormant period, similar to results of (Choudhary et al. 2015). It is understood, that this portlandite is associated with the formation of

amorphous CSH. However, mixture REF 2 should slightly different results. At the beginning, an aluminate reaction with occurrence of ettringite was seen. At the same time, the calcium sulphate source anhydrite decreases, the basanite level stagnates and portlandite arises. Findings of (Nehringa et al. 2018) showed similar findings for the aluminate reaction. Nevertheless, the observed silicate reaction was different to the reaction from the research of (Nehringa et al. 2018). REF 2 reacts faster. portlandite was found approximately during 2.0 and 2.3 hours. (Nehringa et al. 2018) detected it first after 46 hours. Independently from that, the depletion of calcite was seen. It is presumed, that aluminium form the added CAC causes the reaction of calcite. This is in line with the research of (Bizzozero and Scrivener 2015).

Overall, the results showed the significant effects of SCMs on dry-mix shotcrete mixtures. The addition of CAC SC1 led to an increase of the early CS. On the other side, mixtures with CAC PPP did not show such clear behaviour. Mixtures with additional CAL EGU in combination with MIF MET SF showed an increased CS-value at later stages, at about 28 days of hydration. A further influencing factor was the reduced W/B-value in combination with an additional plasticiser. However, the effect was not as high as expected during the very important first few hours. Furthermore, the other constituents have to be considered. In particular, the influence of the compacting energy through the spraying and the addition of other components, for instants the aggregate distribution or the addition of additives, such as plasticizers. In opinion of the author, continuous research should focus on proofing the linear relation between heat release and compressive strength development. In detail, the focus should be on the period during the tenth and eighteenth hour of hydration. In addition to that, the different thermal dynamic behaviour of CAC SC1 and CAC PP222 need to be illuminated. Furthermore, the occurrence of a shoulder (additional peak) during reactions of CAC PP222 should be observed. Independent from previous annotations, the development of new recipes of mixtures should be resumed. Therefore, mixtures W2-11b could be recommended. It showed a well early-age compressive strength development. On top of that, findings in (Thumann and Röck 2017) showed a positive leaching behaviour of the constituent metakaoline, which is part of mixture W2-11b.

List of literature

- Advanced concrete technology*. 2003. Oxford, England: Butterworth-Heinemann. <http://www.sciencedirect.com/science/book/9780750656863>.
- Antoni, M., J. Rossen, F. Martirena, and K. Scrivener. 2012. "Cement substitution by a combination of metakaolin and limestone." *Cement and concrete research* 42 (12): 1579–89. doi:10.1016/j.cemconres.2012.09.006.
- Belie, Nele de, Marios Soutsos, and Elke Gruyaert, eds. 2018. *Properties of Fresh and Hardened Concrete Containing Supplementary Cementitious Materials: State-of-the-Art Report of the RILEM Technical Committee 238-SCM, Working Group 4*. RILEM State-of-the-Art Reports 25. Cham: Springer International Publishing. <http://dx.doi.org/10.1007/978-3-319-70606-1>.
- Benedix, Roland. 2015. *Bauchemie: Einführung in die Chemie für Bauingenieure und Architekten*. 6., vollst. überarb. und aktualisierte Aufl. Lehrbuch. Wiesbaden: Springer Vieweg. <http://dx.doi.org/10.1007/978-3-658-04144-1>.
- Bentz, D. P., T. Barrett, I. de La Varga, and W. J. Weiss. 2012. "Relating Compressive Strength to Heat Release in Mortars." *Advances in Civil Engineering Materials* (1): 1–14.
- Bentz, Dale P., Max A. Peltz, and John Winpiger. 2009. "Early-Age Properties of Cement-Based Materials. II: Influence of Water-to-Cement Ratio." *Journal of Materials in Civil Engineering* 21 (9): 512–17. doi:10.1061/(asce)0899-1561(2009)21:9(512).
- Bentz, Dale P., Gaurav Sant, and Jason Weiss. 2008. "Early-Age Properties of Cement-Based Materials. I: Influence of Cement Fineness." *Journal of Materials in Civil Engineering* 20 (7): 502–8. doi:10.1061/(asce)0899-1561(2008)20:7(502).
- Bizzozero, Julien, and Karen L. Scrivener. 2015. "Limestone reaction in calcium aluminate cement–calcium sulfate systems." *Cement and concrete research* 76: 159–69.
- Briendl, L., J. Juhart, M. Krüger, F. Mittermayr, and I. Galan. 2018. "Early Strength Improvement of Sustainable Shotcrete."
- Choudhary, H. K., A. V. Anupama, R. Kumar, M. E. Panzi, S. Matteppanavar, Baburao N. Sherikar, and B. Sahoo. 2015. "Observation of phase transformations in cement during hydration." *Construction and Building Materials* 101: 122–29.
- Czernin, Wolfgang. 1980. *Cement chemistry and physics for civil engineers*. 2. Engl. ed. Wiesbaden: Bauverlag; Godwin.
- Danielson, U. H. 1962. "Heat of hydration of cement as affected by water–cement ratio." *Proceedings of the 4th International Symposium on the Chemistry of (IV)*: 519–26.
- El-Diadamony, Hamdy, Ahmed A. Amer, Tarek M. Sökkary, and Samir El-Hoseny. 2016. "Hydration and characteristics of metakaolin pozzolanic cement pastes." *HBRC Journal*. doi:10.1016/j.hbrj.2015.05.005.
- El-Hadj Kadria, Said Kenaib, Karim Ezzianec, Rafat Siddiqued, and Geert De Schuttere. 2011. "Influence of metakaolin and silica fume on the heat of hydration and compressive strength development of mortar." *Applied Clay Science* (53): 704–8.
- Feldman, R. F., and Huang Cheng-yi. 1985. "Properties of portland cement-silica fume pastes II. Mechanical properties." *Cement and concrete research*, 943–52. doi:10.1016/0008-8846(85)90083-3.

- Frias, M., and J. Cabrera. 2000. "Pore size distribution and degree of hydration of metakaolin-cement pastes." *Cement and concrete research* 1999 (30): 561–69.
- Hewlett, P. C., and Frederick Lea, eds. 2001. *Lea's chemistry of cement and concrete*. 4. ed., repr. London: Arnold.
- Jiong Hu, Zhi Ge, and Kejin Wang. "Influence of cement fineness and water-to-cement ratio on mortar early-age heat of hydration and set times." *Construction and Building Materials* 2014 (50): 657–63. <http://www.sciencedirect.com/science/article/pii/S0950061813009215>.
- Juhart J., Briendl L., Sakoparnig M., Thumann M., Steindl F., Röck R., Mittermayr F., and Kusterle W. 2018. *Forschungsprojekt ASSpC: Bericht Trockenspritzbeton*. Wietersdorf 12.3 - 16.3.2018.
- Kim, J.-K, Y.-H Moon, and S.-H Eo. 1998. "Compressive strength development of concrete with different curing time and temperature." *Cement and concrete research* 28 (12): 1761–73. doi:10.1016/S0008-8846(98)00164-1.
- Krischner, Harald, and Brigitte Koppelhuber-Bitschnau. 1994. *Röntgenstrukturanalyse und Rietveldmethode: Eine Einführung*. 5., neubearbeitete Auflage. Wiesbaden: Vieweg+Teubner Verlag. <http://dx.doi.org/10.1007/978-3-663-12348-4>.
- Krstulović, P., N. Kamenić, and K. Popović. 1994. "A new approach in evaluation of filler effect in cement: I. Effect on strength and workability of mortar and concrete." *Cement and concrete research* (vol. 24 (4)): 721–27.
- Kusterle, Wolfgang, ed. 2006. *Spritzbeton-Technologie 2006: Berichtsband der 8. internationalen Fachtagung, Alpbach, 26. + 27. Januar 2006 = Shotcrete technology 2006 ; papers presented at the 8th conference*. Innsbruck: Univ. Inst. für Betonbau Baustoffe und Bauphysik.
- Le Puerta-Falla, Guillermo a. B. M. a. S. G. a. N. N. a. S. G. 2015. "The Influence of Metakaolin on Limestone Reactivity in Cementitious Materials." In *Calcined Clays for Sustainable Concrete*, edited by Karen a. F. A. Scrivener, 11–19. Dordrecht: Springer Netherlands.
- Marsh, B. K., R. L. Day, and D. G. Bonner. 1985. "Pore structure characteristics affecting the permeability of cement paste containing fly ash." *Cement and concrete research* 15 (6): 1027–38. doi:10.1016/0008-8846(85)90094-8.
- Matschei, T., B. Lothenbach, and F. P. Glasser. 2007. "The role of calcium carbonate in cement hydration." *Cement and concrete research* 37 (4): 551–58. doi:10.1016/j.cemconres.2006.10.013.
- Nehringa, J., J. Neubauer, S. Bergerb, and Goetz-Neunhoeffler F. 2018. "Acceleration of OPC by CAC in binary and ternary systems - The role of pore solution chemistry." *Cement and concrete research* (107): 264–74.
- ÖNORM EN 14488-2. 2006. *Testing sprayed concrete – Part 2: Compressive strength of young sprayed concrete* 91.100.30. Heinestraße 38, 1020 Wien: Austrian Standards Institute.
- ÖNORM EN 196-1: 2016 10 15. 2016. *Methods of testing cement — Part 1: Determination of strength* 91.100.10. Heinestraße 38, 1020 Wien: Austrian Standards Institute.
- Poso, Antti, and Björn Windshügel. 2014. *Beton-Kalender 2014: Schwerpunkte: Unterirdisches Bauen ; Grundbau ; Eurocode 7*. 2. Aufl. Beton-Kalender (VCH) *. s.l. Ernst Sohn. <http://gbv.ebib.com/patron/FullRecord.aspx?p=1732303>.
- Reschke, T., E. Siebel, and G. Thielen. 1999. "Einfluß der Granulometrie und Reaktivität von Zement und Zusatzstoffen auf die Festigkeits- und Gefügeentwicklung von Mörtel und Beton." *beton* 49 1999 (12): 719–24.

- Richtlinie "Spritzbeton"*. 2009. Wien: Österreichische Vereinigung für Beton- und Bautechnik. Schriftenreihe / Österreichische Bautechnik Vereinigung.
- Ruffert, Günter, Gunther Brux, and Hans-Joachim Badzong. 1995. *Spritzbeton: Herstellung, Prüfung und Anwendung von Spritzbeton ; Abwicklung von Spritzbetonarbeiten ; Sondergebiete einschliesslich Faserspritzbeton ; Schutz und Instandsetzung von Bauwerken*. Kontakt & Studium Baupraxis 348. Renningen-Malmsheim: expert-Verl.
- Salvador, Renan P., Sergio H. P. Cavalaro, Miguel Cano, and Antonio D. Figueiredo. 2016. "Influence of spraying on the early hydration of accelerated cement pastes." *Cement and concrete research* 88: 7–19.
- Schutter, G., and Taerwe L. de. 1996. "Degree of hydration-based description of mechanical properties of early age concrete." *Materials and Structures* 29 (6): 335. doi:10.1007/BF02486341.
- Scrivener, Karen. 2003. "2 - Calcium aluminate cements." In *Advanced Concrete Technology*, edited by John Newman and Ban S. Choo, 1–31. Oxford: Butterworth-Heinemann.
- Scrivener, Karen, Ruben Snellings, and Barbara Lothenbach, eds. 2016. *A practical guide to microstructural analysis of cementitious materials*. A Spon Press Book. Boca Raton: CRC Press Taylor & Francis Group.
- Shuang Zhang, Jing, Qin Yong Ma, and Xing Teng Han. 2010. "Experimental Research on Compressive Strength and Storage Period for Dry-Mixed Material of Shotcrete." *Advanced Materials Research* 168-170.
- Speakman, S. A. "Basics of X-Ray Powder Diffraction: Training to Become an Independent User of the X-Ray SEF at the Center for Materials Science and Engineering at MIT." Accessed 09/18. <http://prism.mit.edu/xray/Basics%20of%20X-Ray%20Powder%20Diffraction.pdf>.
- Springenschmid, Rupert. 2007. *Betontechnologie für die Praxis*. 1. Aufl. Berlin: Bauwerk. http://deposit.d-nb.de/cgi-bin/dokserv?id=2895996&prov=M&dok_var=1&dok_ext=htm.
- Stark, Jochen, and Bernd Wicht. 2000. *Zement und Kalk: Der Baustoff als Werkstoff*. BauPraxis. Basel: Birkhäuser Basel. <http://dx.doi.org/10.1007/978-3-0348-8382-5>.
- Taylor, Harry F. W. 2003. *Cement chemistry*. 2. ed., repr. London: Telford Publ.
- Thumann, and Röck. 2017. *Spritz-Bindemittel: Bericht über Vorversuche und Trockenspritzversuche Spritz- Bindemittel*.
- Wegmüller, Marcel C. 2001. *Einflüsse des Bergwassers auf Tiefbau*. Zürich: Stäubli.
- Zement-Taschenbuch*. 2008. 51. Aufl. Zement-Taschenbuch 51. Düsseldorf: Verlag Bau + Technik.

List of Illustration

Figure 1: Dry-mix procedure, adapted from (Ruffert, Brux, and Badzong 1995).....	8
Figure 2: Typical hydration kinetics of pure clinker minerals (C_3A without and with added gypsum)	10
Figure 3: Example of heat of hydration curve of an OPC 1: initial endothermic peak; 2: initial exothermic peak; 3: inflection point (dormant period ends); 4: peak of acceleration period; 5: AFt formation; 6: conversion of AFt to AFm.....	15
Figure 4: Pore- Distribution as a function of w/c ratio.....	16
Figure 5: Composition range of CAC compared with OPC	18
Figure 6: Reaction of OPC with H (left) in comparison with CAC with H (right)	18
Figure 7: Schematic illustration of an isothermal calorimeter.....	21
Figure 8: Basic example of a Bravais lattice	22
Figure 9: Bragg diffraction from a cubic crystal lattice	23
Figure 10: Example of a XRD-analysis.....	24
Figure 11: Grain-size-curve of the aggregate, which was used at the full-scale test	28
Figure 12: Experimental arrangement: 1: Powder actuated nail gun; 2: Nail; 3: Nail with a washer and an unscrewed head; 4: removing device	30
Figure 13: Mixtures with its components	31
Figure 14: Grain-size-curve of used aggregate in the laboratory tests.....	32
Figure 15: Compressive Strength-testing machine "ToniNORM" (300kN)	34
Figure 16: Bending tensional-testing machine "ToniNORM" (10kN).....	34
Figure 17: Compressive strength-testing machine "SHIMADZU AUTOGRAPH AG-50kNG" (50kN)	34
Figure 18: Calorimeter "I-Cal 4000 HPC"	35
Figure 19: Inside look of isothermal test units	35
Figure 20: XRD chamber.....	36
Figure 21: XRD-machine.....	36
Figure 22: Results from CS-tests at 6h, 24h and 28d.....	37
Figure 23: Results from CS-tests at 1h, 3h, 6h, 24h and 28d.....	38
Figure 24: Heat of hydration of dry-mix shotcrete mortar with CEM I 52,5N SRO.....	39
Figure 25: Cumulative heat of hydration of dry-mix shotcrete mortars with CEM I 52,5N SRO and other SCMs.....	39
Figure 26: Heat of hydration of dry-mix shotcrete mortars with SPBM2 and other SCMs	40
Figure 27: Cumulative heat of hydration of dry-mix shotcrete mortars containing SPBM2 and other SCMs	41
Figure 28: Heat of hydration of dry-mix shotcrete mortars with 100% SPBM2 and different sample sizes	42
Figure 29: Cumulative heat of hydration of dry-mix shotcrete mortars containing 100% SPBM2 and different sample sizes	42

Figure 30: Heat of hydration of dry-mix shotcrete mortars with 90% CEM I 52.5N SRO with 10% CAC SC1 and different sample sizes.....	43
Figure 31: Cumulative heat of hydration of dry-mix shotcrete mortars containing 90% CEM 52.5N SRO with 10% CAC SC1 and different sample sizes.....	44
Figure 32: XRD-patterns of REF 1.....	45
Figure 33: 24h in-situ XRD 3D-plot from 9-50 2θ° (Co) of mixture REF1.....	46
Figure 34: 24h in-situ XRD 2D-plot from 9-50° 2θ (Co) of mixture REF1.....	46
Figure 37: XRD-patterns of REF 2.....	47
Figure 35: 24h in-situ XRD 3D-plot from 9-50° 2θ (Co) of mixture REF2.....	48
Figure 36: 24h in-situ XRD 2D-plot from 9-50° 2θ (Co) of mixture REF2.....	48
Figure 38: Samples which was made in the laboratory.....	51
Figure 39: Cylindrical sample cut out from a sample produced at the full-scale test.....	51
Figure 40: Initial peaks of mixtures with SPBM2.....	53
Figure 41: Initial peaks of mixtures wit CEM I SRO.....	53
Figure 42: Heat Release vs. Compressive Strength of all tested samples.....	54
Figure 43: Heat Release vs. Compressive Strength of tested mortars consists of 100% SPBM2.....	55
Figure 44: Heat Release vs. Compressive Strength of tested mortars consists of 90% CEM I SRO and 10% CAC SC1.....	55
Figure 45: Intensity trends during the ongoing hydration of REF1.....	57
Figure 46: Intensity trends during the ongoing hydration of REF2.....	57

List of Tables

Table 1: C ₃ A/CsH ₂ - ratio and predicted reaction products	12
Table 2: Summarized stages of the hydration process	14
Table 3: Overview of the experimental programme	25
Table 4: List of raw materials that was used in Wietersdorf 2018	26
Table 5: Base material for laboratory experiments	26
Table 6: Chemical components of base materials	27
Table 7: Mineralogical components of base materials	27
Table 8: Blends from the full-scale test in Wietersdorf.....	29
Table 8: Compressive strength results from the full- scale test	30
Table 10: Mixtures produced in the laboratory	31
Table 11: Machine specifications	33
Table 12: CS-results of samples W2-03 to W2-14 with sample standard deviation (SSD).....	38
Table 13: CS-results of samples REF 1 and REF 2 with SSD	38
Table 14: Summary of the hydration periods of dry-mix shotcrete mortars with CEM I 52,5N SRO and SCMs.....	40
Table 15: Summary of the hydration periods of dry-mix shotcrete mortar with SPBM2 and SCMs.....	41
Table 16: Summary of the hydration periods of dry-mix shotcrete mortar with 100% SPBM2	43
Table 17: Summary of the hydration periods of dry- mix shotcrete mortar with 90% CEM I 52,5N SRO and 10% CAC-SC1	44
Table 18: Findings of the in-situ XRD investigations of mixtures with 100% SPBM2	46
Table 19: Findings of the in-situ XRD investigations of mixtures with 90% CEM I SRO and 10% CAC SC1	48
Table 20: Comparison of full-scale-test-results with results from the laboratory tests.....	51
Table 21: Heat release by phase and heat release by time for each phase of hydration.....	52
Table 22: Comparison of cumulative heat progresses	53
Table 23: Sample characteristics after one hour.....	66
Table 24: Sample characteristics after three hours	66
Table 25: Sample characteristics after six hour	66
Table 26: Sample characteristics after 24 hours	67
Table 27: Sample characteristics after 28 days.....	67

Appendix A

Sample Characteristic:

Sample:	Mass [g]	Length [mm]	Width [mm]	Height [mm]
REF-1-03	561.3	160.20	39.50	40.90
REF-1-04	571.6	160.05	39.85	40.05
REF-2-03	559.9	159.96	40.45	40.12
REF-2-04	564.7	160.18	40.44	39.95

Table 23: Sample characteristics after one hour

Sample:	Mass [g]	Length [mm]	Width [mm]	Height [mm]
REF-1-03	566.8	160.12	39.85	40.10
REF-1-04	563.4	159.98	40.35	40.05
REF-2-03	561.4	160.87	40.63	39.94
REF-2-04	565.2	161.14	40.57	39.99

Table 24: Sample characteristics after three hours

Sample:	Mass [g]	Length [mm]	Width [mm]	Height [mm]
W2-03-01	572.3	160.36	40.98	40.13
W2-03-02	566.8	160.63	40.68	40.26
W2-04-01	564.2	160.10	40.69	40.16
W2-04-02	561.7	160.01	40.65	40.14
W2-10-01	556.8	160.21	40.87	40.09
W2-10-02	548.8	160.07	40.36	40.08
W2-11-01	546.1	160.12	40.20	40.17
W2-11-02	550.1	159.60	40.06	40.13
W2-12-01	547.3	160.65	40.21	40.19
W2-12-02	539.9	159.98	40.10	40.08
W2-13-01	580.8	160.65	40.51	40.22
W2-13-02	567.0	160.18	40.09	40.19
W2-14-01	544.5	160.25	40.08	40.45
W2-14-02	535.1	159.89	40.23	39.98
REF-1-01	551.1	160.16	40.03	40.11
REF-1-02	547.7	160.24	40.38	40.23
REF-2-01	568.2	160.25	40.20	39.96
REF-2-02	569.2	160.31	40.14	40.13

Table 25: Sample characteristics after six hour

Sample:	Mass [g]	Length [mm]	Width [mm]	Height [mm]
W2-03-01	566.2	160.37	40.51	40.29
W2-03-02	564.2	160.29	40.99	40.37
W2-04-01	561.4	160.01	40.43	40.14
W2-04-02	562.0	160.31	41.20	40.22
W2-10-01	553.7	160.22	40.94	40.13
W2-10-02	543.7	160.07	40.20	39.96
W2-11-01	551.5	160.13	40.06	40.12
W2-11-02	551.5	160.57	40.17	40.02
W2-12-01	540.1	160.20	40.33	40.04
W2-12-02	540.6	160.00	40.37	40.11
W2-13-01	574.2	160.46	40.20	40.13
W2-13-02	561.8	160.34	40.59	40.02
W2-14-01	543.4	160.31	40.65	40.04
W2-14-02	534.9	160.27	40.07	40.02
REF-1-01	552.5	160.19	40.07	39.66
REF-1-02	549.0	160.25	40.19	40.12
REF-2-01	565.2	160.29	40.30	40.15
REF-2-02	563.9	160.39	40.49	40.24

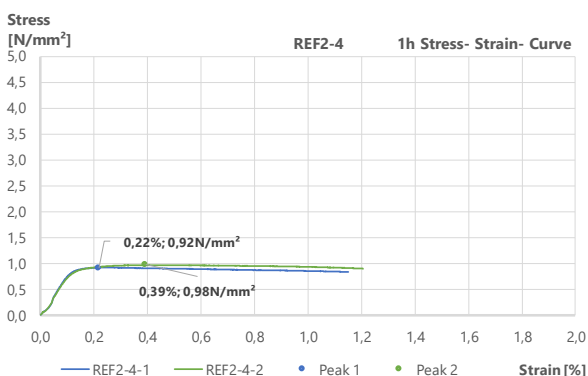
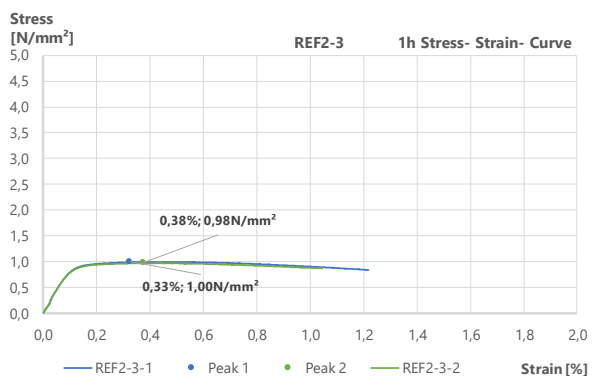
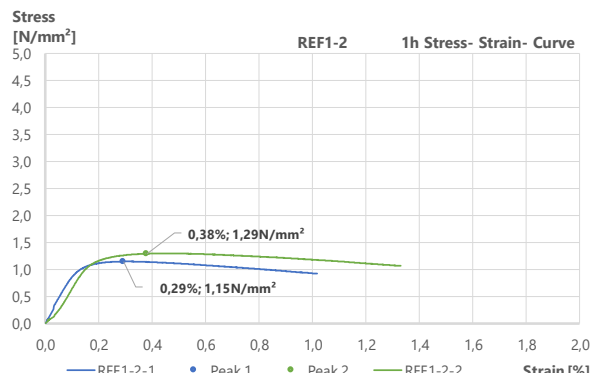
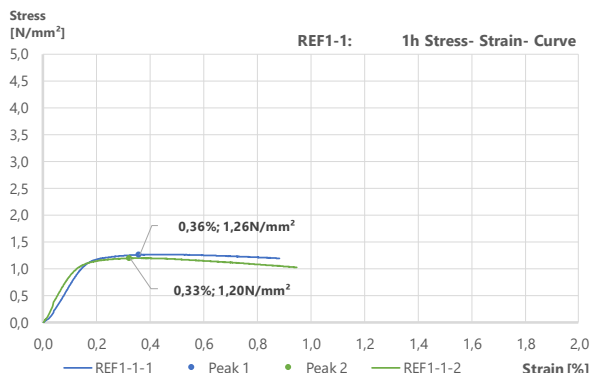
Table 26: Sample characteristics after 24 hours

Sample:	Mass [g]	Length [mm]	Width [mm]	Height [mm]
W2-03-01	564.9	160.30	40.42	40.70
W2-03-02	570.3	160.36	40.96	41.13
W2-04-01	565.5	160.90	40.27	40.65
W2-04-02	556.1	160.13	40.08	40.33
W2-10-01	559.0	160.30	40.35	41.04
W2-10-02	549.4	160.53	40.06	40.59
W2-11-01	551.5	160.13	40.56	40.19
W2-11-02	562.9	160.05	40.26	40.39
W2-12-01	548.0	160.16	40.10	40.18
W2-12-02	557.9	160.07	40.81	40.49
W2-13-01	565.7	160.19	39.96	40.50
W2-13-02	562.9	160.20	39.93	40.10
W2-13-03	571.2	160.31	40.54	40.39
W2-14-01	561.5	160.15	40.65	40.12
W2-14-02	561.8	160.13	40.45	40.14
W2-14-03	564.1	160.34	40.44	40.20
REF-1-01	560.9	160.36	40.13	40.20
REF-1-02	557.8	160.34	40.30	40.28
REF-2-01	570.4	160.36	40.48	40.37
REF-2-02	568.6	160.34	40.37	40.12

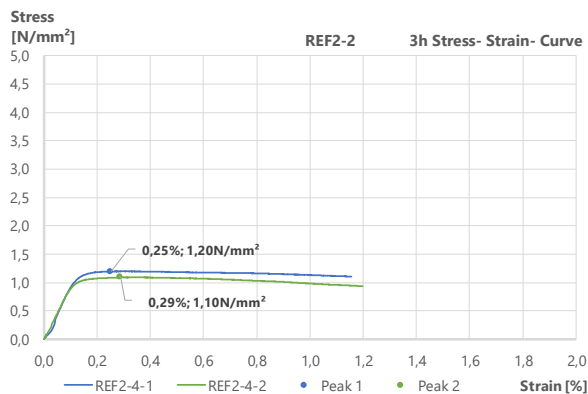
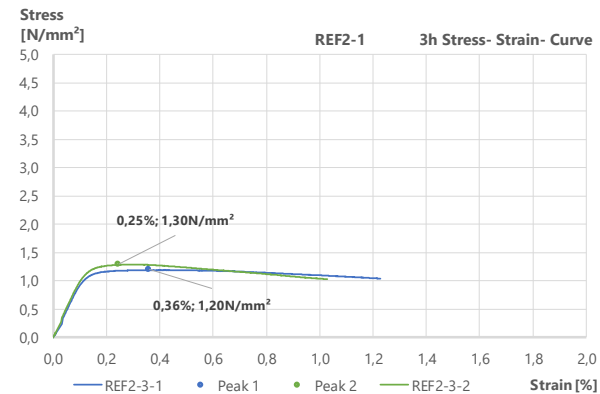
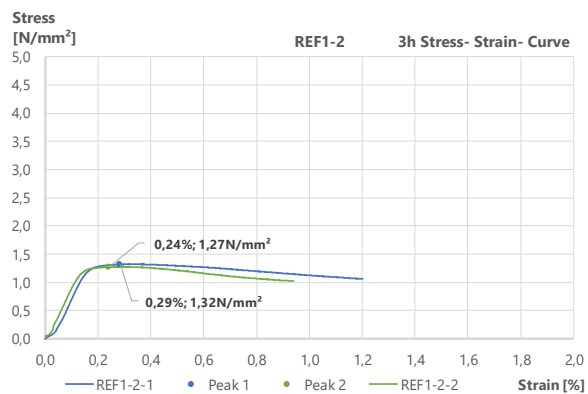
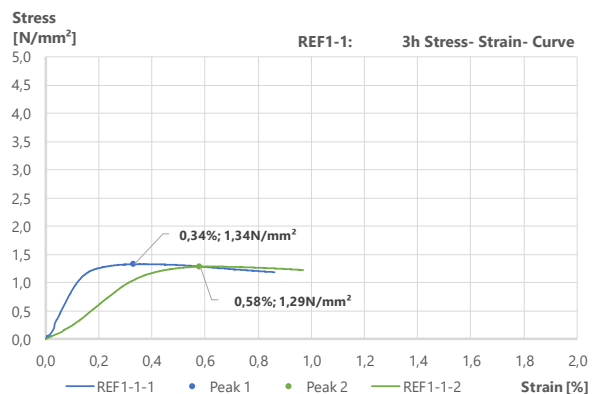
Table 27: Sample characteristics after 28 days

Appendix B

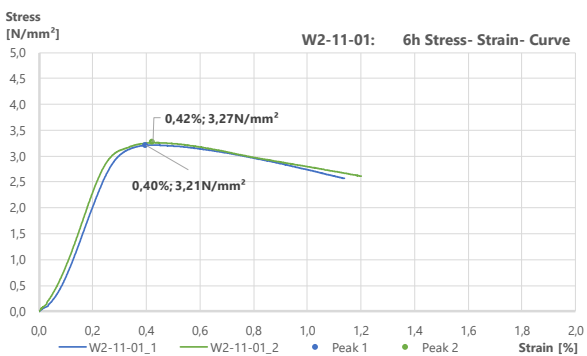
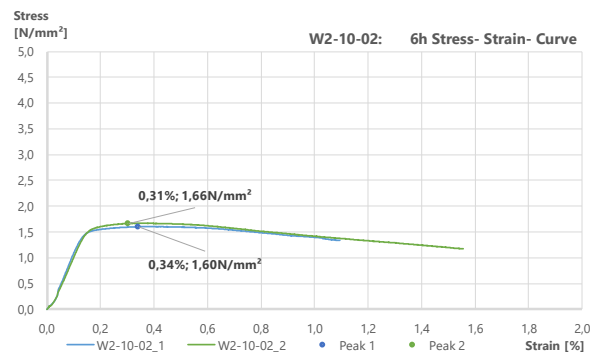
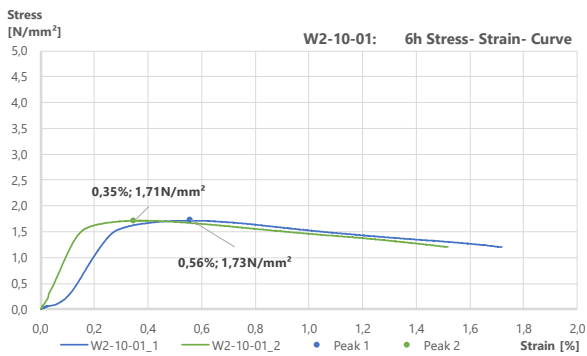
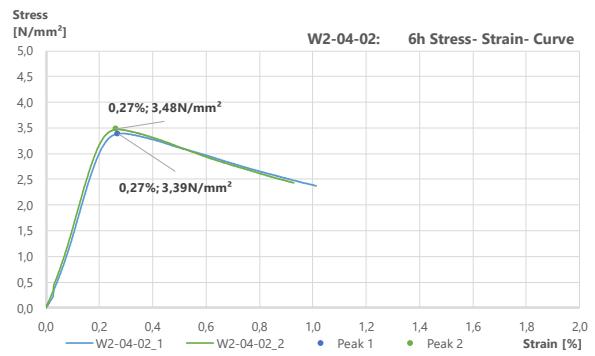
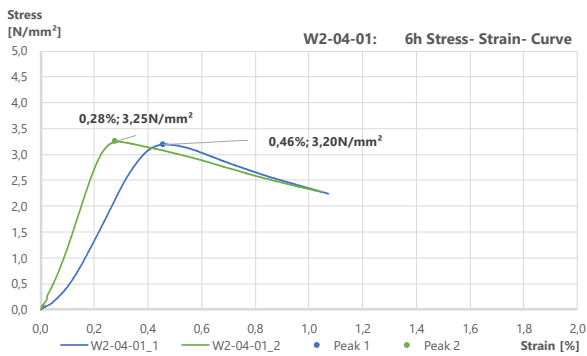
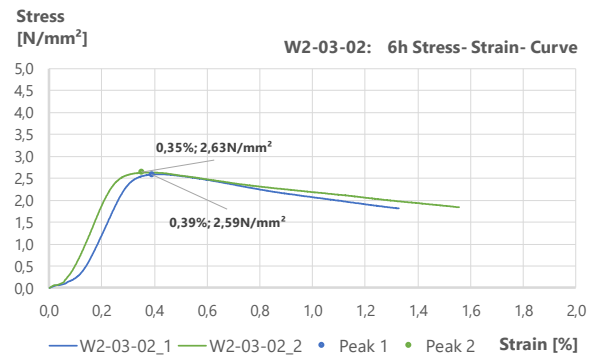
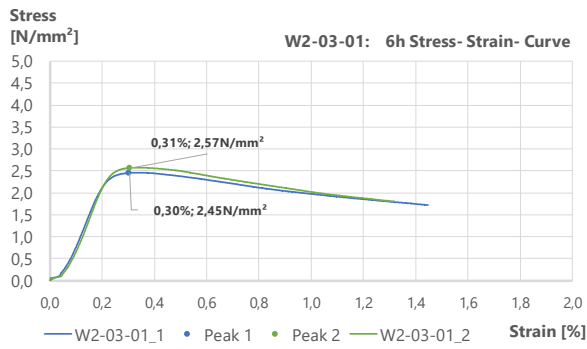
CS- results 1h:

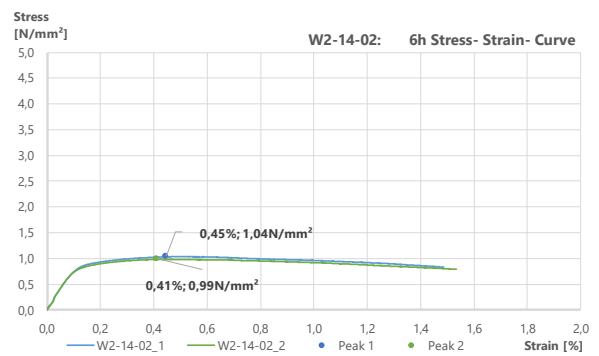
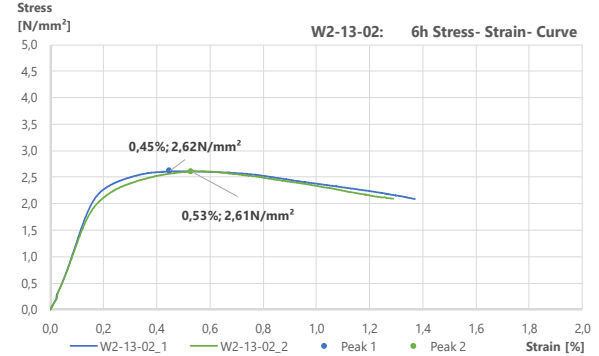
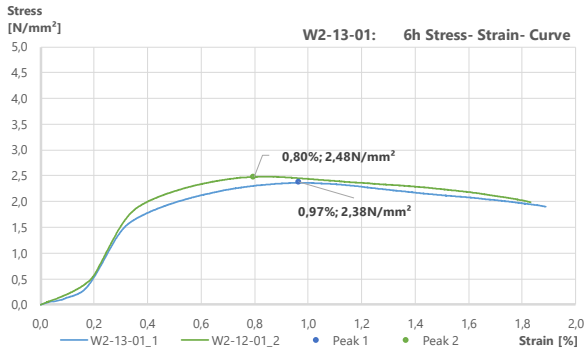
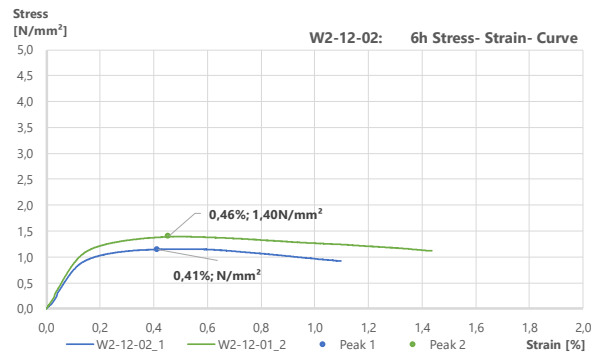
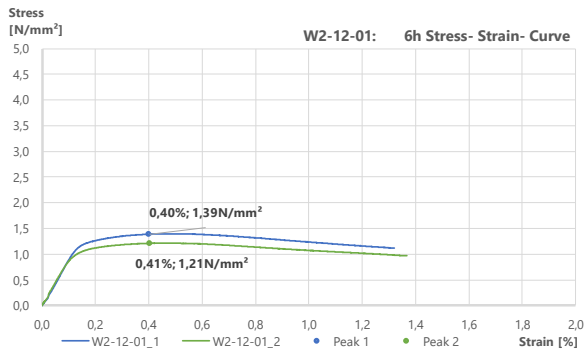


CS- results 3h:

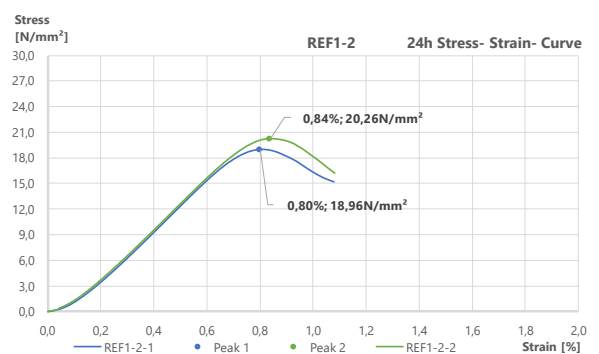
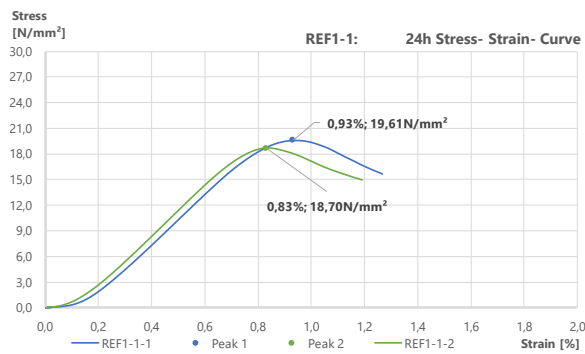


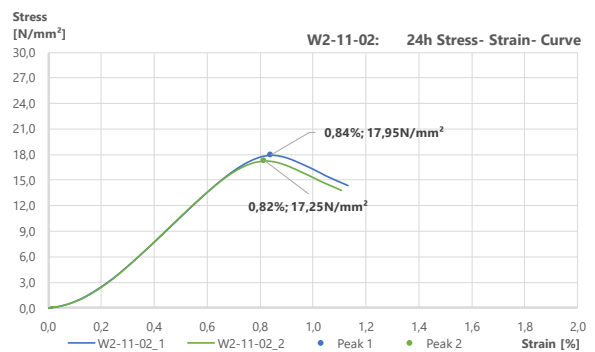
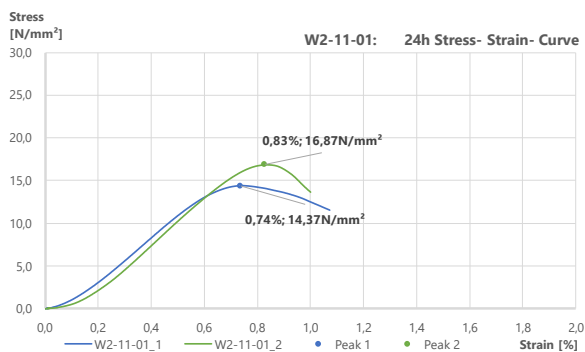
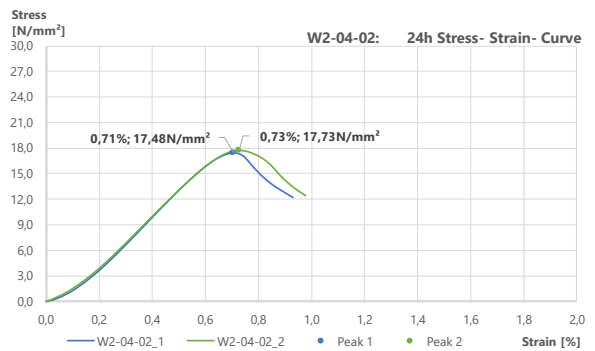
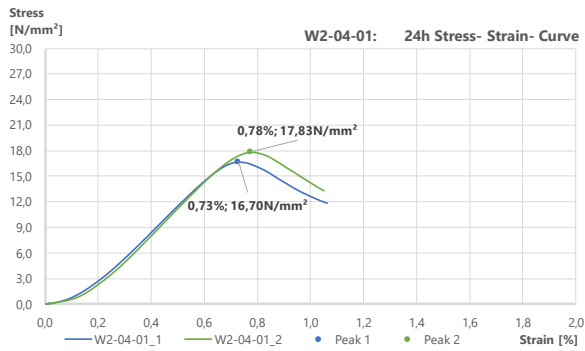
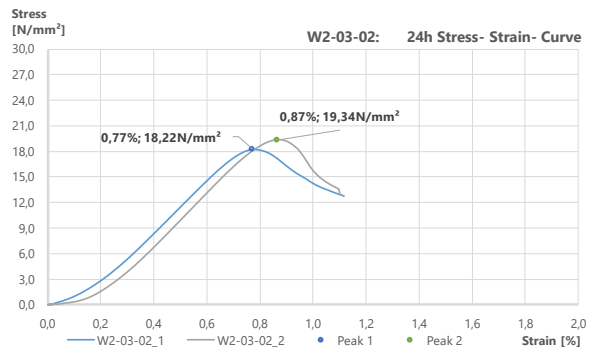
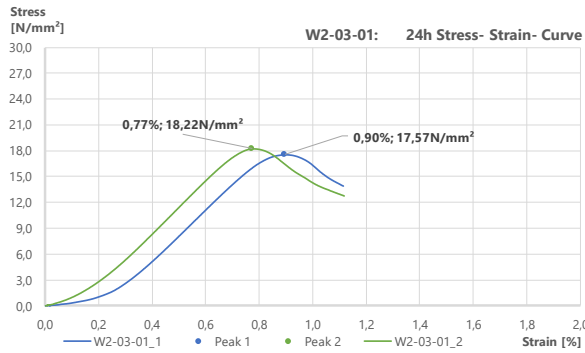
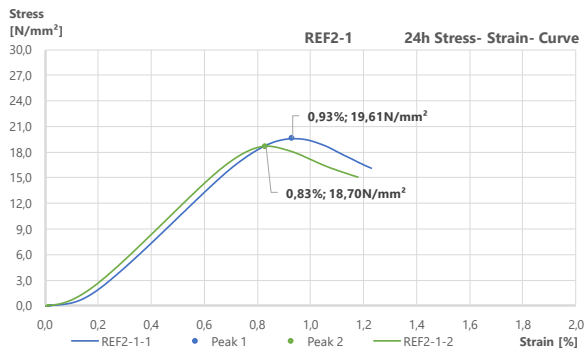
CS- results 6h:





CS- results 24h:







Appendix C

Power- and heat curves:

